Supplementary Information for

Activating charge-transfer state formation in strongly coupled dimers using DNA scaffolds

Stephanie M. Hart[1,§], James L. Banal[2,§], Maria A. Castellanos[1,§], Larysa Markova[3], Yuliia Vyborna[3], Jeffrey Gorman[2], Robert Häner[3], Adam P. Willard[1,*], Mark Bathe[2,*], and Gabriela S. Schlau-Cohen[1,*]

[1]Department of Chemistry, Massachusetts Institute of Technology, Cambridge, MA 02139 USA
[2]Department of Biological Engineering, Massachusetts Institute of Technology, Cambridge, MA 02139 USA
[3]Department of Chemistry, Biochemistry and Pharmaceutical Sciences, University of Bern, Freiestrasse 3, CH-3012, Bern, Switzerland

* Correspondence should be addressed to: awillard@mit.edu (A.P.W.), mark.bathe@mit.edu (M.B.), gssc@mit.edu (G.S.S.C.)
§These authors contributed equally.

Contents

List of Figures

List of Tables

S1 General methods

Equimolar concentrations of canonical single-stranded DNA (ssDNA) and squaraine-modified ssDNA were hybridized in 1× phosphate-buffered saline (PBS, 137 mM NaCl, 10 mM phosphate, 2.7 mM KCl) solution using a linear temperature ramp: 95 °C for 5 minutes then 80–20 °C at −1 °C min^{-1}. Hybridized double-stranded DNA (dsDNA) constructs were kept at 4 °C until further use. Sample absorbance and fluorescence spectra were measured using an Evolution 260 Bio UV-Vis spectrophotometer (Thermo Fisher) and Fluoromax-4C (Horiba Jobin Yvon), respectively, unless otherwise stated. Cuvette-based measurements were performed using 10-mm pathlength quartz micro cuvettes (Millipore Sigma, catalog number: Z802662). For Fluoromax-4C measurements, all fluorescence spectra were corrected for wavelength-dependent lamp output and detector sensitivity ('S1c/R1c' detector setting). The sample absorbances at the maximum absorbance peaks of all samples were kept at 0.1 or less for all fluorescence measurements to avoid inner filter effects.

S1.1 DNA sequences

Table S1. Squaraine-modified and canonical ssDNA sequences (**X** denotes internal squaraine modification).

Sequence identifier	ssDNA sequence (5' to 3' direction)
Chromophore Monomer ssDNA	AGCTCGGTCA**X**CGAGAGTGCA
Chromophore Serial Δ0 ssDNA	AGCTCGGTCA**XX**CGAGAGTGCA
Chromophore Serial Δ1 ssDNA	AGCTCGGTCA**X**T**X**CGAGAGTGCA
Chromophore Serial Δ2 ssDNA	AGCTCGGTCA**X**TT**X**CGAGAGTGCA
Chromophore Serial Δ3 ssDNA	AGCTCGGTCA**X**TTT**X**CGAGAGTGCA
Chromophore Parallel Δ0 ssDNA A	AGCTCGGTCA**X**CGAGAGTGCA
Chromophore Parallel Δ0 ssDNA B	TGCACTCTCG**X**TGACCGAGCT
Chromophore Parallel Δ1 ssDNA A	AGCTCGGTCA**X**TCGAGAGTGCA
Chromophore Parallel Δ1 ssDNA B	TGCACTCTCG**X**ATGACCGAGCT
Chromophore Parallel Δ2 ssDNA A	AGCTCGGTCA**X**TTCGAGAGTGCA
Chromophore Parallel Δ2 ssDNA B	TGCACTCTCG**X**AATGACCGAGCT
Complementary Monomer ssDNA	TGCACTCTCGATGACCGAGCT
Complementary Serial Δ0 ssDNA	TGCACTCTCGAATGACCGAGCT
Complementary Serial Δ1 ssDNA	TGCACTCTCGATATGACCGAGCT
Complementary Serial Δ2 ssDNA	TGCACTCTCGATTATGACCGAGCT
Complementary Serial Δ3 ssDNA	TGCACTCTCGATTTATGACCGAGCT
Complementary Stem loop-1 ssDNA	TGCACTCTCGCGCTTTTGCGTGACCGAGCT
Complementary Stem loop-2 ssDNA	TGCACTCTCGCGCTTTTGCGTTTCCCTTTTGGGTGACCGAGCT
Complementary Stem loop-3 ssDNA	TGCACTCTCGCGCTTTTGCGTTTCCCTTTTGGGTTTCCGTTTTCGGTGACCGAGCT
Canonical control ssDNA A	AGCTCGGTCATCGAGAGTGCA
Canonical control ssDNA B	TGCACTCTCGTTGACCGAGCT

Table S2. Squaraine-modified dsDNA and constructs. Asterisk (*) denotes construct only examined using high-throughput characterization shown in Figure 2C in the Main Text. Constructs further investigated using ultrafast spectroscopy have bold and italicized construct identifiers. The (comp) notation denotes complementary strands that do not contain a squaraine modification. Relative quantum yields (Φ_F) were calculated according to Eq. S17.

Construct identifier	**ssDNA strand 1**	**ssDNA strand 2**	**Relative Φ_F**
Monomer	Chromophore Monomer	Complementary Monomer	1.000
* Monomer-Serial Δ0 (comp)	Chromophore Monomer	Complementary Serial Δ0	1.050
* Monomer-Serial Δ1 (comp)	Chromophore Monomer	Complementary Serial Δ1	0.960
* Monomer-Serial Δ2 (comp)	Chromophore Monomer	Complementary Serial Δ2	1.110
* Monomer-Serial Δ3 (comp)	Chromophore Monomer	Complementary Serial Δ3	1.290
* Monomer-Stem loop-1 (comp)	Chromophore Monomer	Complementary Stem loop-1	1.890
* Monomer-Stem loop-2 (comp)	Chromophore Monomer	Complementary Stem loop-2	1.210
Stem loop-3 Monomer	Chromophore Monomer	Complementary Stem loop-3	1.280
Serial Δ0 ***Dimer***	Chromophore Serial Δ0	Complementary Serial Δ0	0.005
* Serial Δ0-Serial Δ1 (comp)	Chromophore Serial Δ0	Complementary Serial Δ1	0.005
* Serial Δ0-Serial Δ2 (comp)	Chromophore Serial Δ0	Complementary Serial Δ2	0.005
* Serial Δ0-Serial Δ3 (comp)	Chromophore Serial Δ0	Complementary Serial Δ3	0.005
* Serial Δ0-Monomer (comp)	Chromophore Serial Δ0	Complementary Monomer	0.005
* Serial Δ0-Stem loop-1 (comp)	Chromophore Serial Δ0	Complementary Stem loop-1	0.004
* Serial Δ0-Stem loop-2 (comp)	Chromophore Serial Δ0	Complementary Stem loop-2	0.010
* Serial Δ0-Stem loop-3 (comp)	Chromophore Serial Δ0	Complementary Stem loop-3	0.010
Serial Δ1 ***Dimer***	Chromophore Serial Δ1	Complementary Serial Δ1	0.006
* Serial Δ1-Serial Δ0 (comp)	Chromophore Serial Δ1	Complementary Serial Δ0	0.005
* Serial Δ1-Serial Δ2 (comp)	Chromophore Serial Δ1	Complementary Serial Δ2	0.007
* Serial Δ1-Serial Δ3 (comp)	Chromophore Serial Δ1	Complementary Serial Δ3	0.005
* Serial Δ1-Monomer (comp)	Chromophore Serial Δ1	Complementary Monomer	0.004
* Serial Δ1-Stem loop-1 (comp)	Chromophore Serial Δ1	Complementary Stem loop-1	0.006
* Serial Δ1-Stem loop-2 (comp)	Chromophore Serial Δ1	Complementary Stem loop-2	0.030
Stem loop-3 Δ1 ***Dimer***	Chromophore Serial Δ1	Complementary Stem loop-3	0.070
Serial Δ2 ***Dimer***	Chromophore Serial Δ2	Complementary Serial Δ2	0.008
* Serial Δ2-Serial Δ0 (comp)	Chromophore Serial Δ2	Complementary Serial Δ0	0.005
* Serial Δ2-Serial Δ1 (comp)	Chromophore Serial Δ2	Complementary Serial Δ1	0.007
* Serial Δ2-Serial Δ3 (comp)	Chromophore Serial Δ2	Complementary Serial Δ3	0.008
* Serial Δ2-Monomer (comp)	Chromophore Serial Δ2	Complementary Monomer	0.003
* Serial Δ2-Stem loop-1 (comp)	Chromophore Serial Δ2	Complementary Stem loop-1	0.004
* Serial Δ2-Stem loop-2 (comp)	Chromophore Serial Δ2	Complementary Stem loop-2	0.070
Stem loop-3 Δ2 ***Dimer***	Chromophore Serial Δ2	Complementary Stem loop-3	0.140
Serial Δ3 ***Dimer***	Chromophore Serial Δ3	Complementary Serial Δ3	0.010
* Serial Δ3-Serial Δ0 (comp)	Chromophore Serial Δ3	Complementary Serial Δ0	0.005
* Serial Δ3-Serial Δ1 (comp)	Chromophore Serial Δ3	Complementary Serial Δ1	0.009
* Serial Δ3-Serial Δ2 (comp)	Chromophore Serial Δ3	Complementary Serial Δ2	0.009
* Serial Δ3-Monomer (comp)	Chromophore Serial Δ3	Complementary Monomer	0.003
* Serial Δ3-Stem loop-1 (comp)	Chromophore Serial Δ3	Complementary Stem loop-1	0.005
* Serial Δ3-Stem loop-2 (comp)	Chromophore Serial Δ3	Complementary Stem loop-2	0.120
Stem loop-3 Δ3 ***Dimer***	Chromophore Serial Δ3	Complementary Stem loop-3	0.180
Parallel Δ0 ***Dimer***	Chromophore Parallel Δ0 A	Chromophore Parallel Δ0 B	0.030
Parallel Δ1 ***Dimer***	Chromophore Parallel Δ1 A	Chromophore Parallel Δ1 B	0.020
Parallel Δ2 ***Dimer***	Chromophore Parallel Δ2 A	Chromophore Parallel Δ2 B	0.023

S1.2 Analytical characterization of squaraine-DNA strands

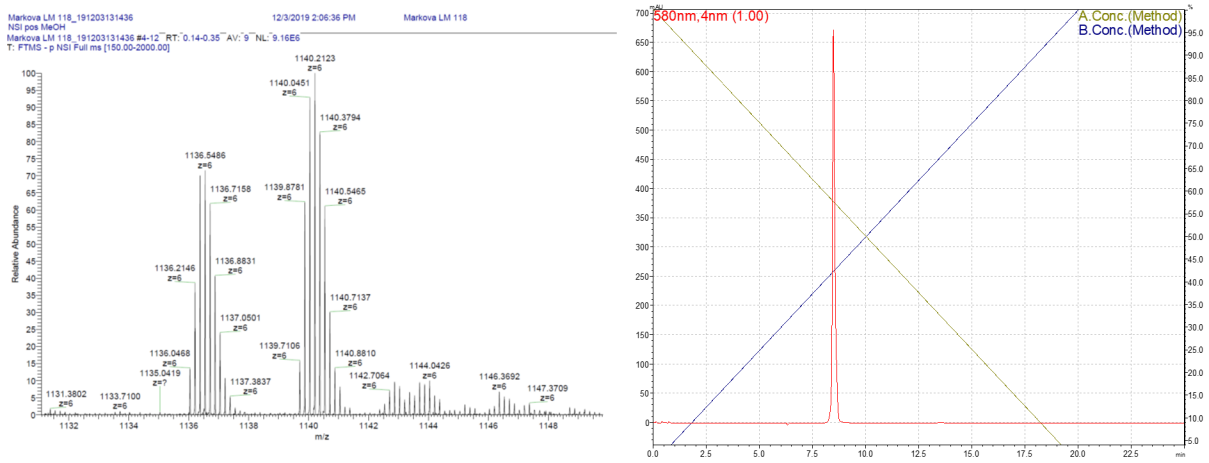

Figure S1. Analytical characterization of squaraine chromophore monomer ssDNA. Left: nanoelectrospray ionization mass spectrum. Right: high performance liquid chromatogram.

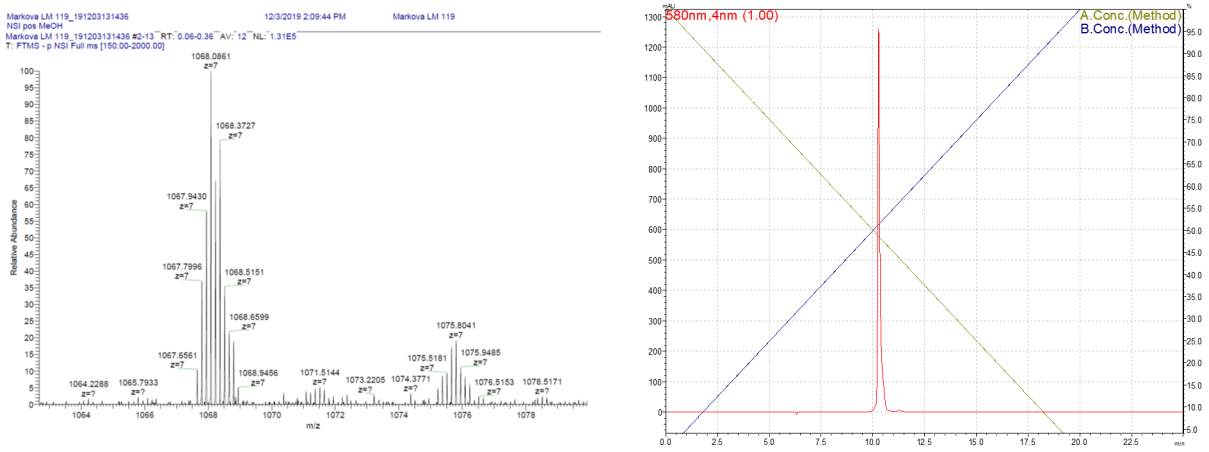

Figure S2. Analytical characterization of chromophore serial $\Delta 0$ ssDNA. Left: nanoelectrospray ionization mass spectrum. Right: high performance liquid chromatogram.

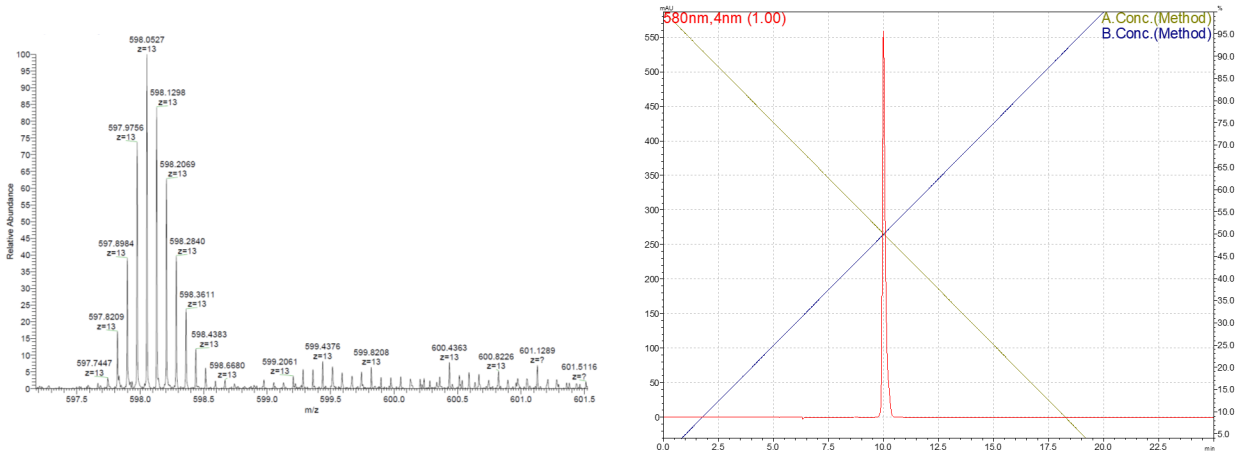

Figure S3. Analytical characterization of chromophore serial $\Delta 1$ ssDNA. Left: nanoelectrospray ionization mass spectrum. Right: high performance liquid chromatogram.

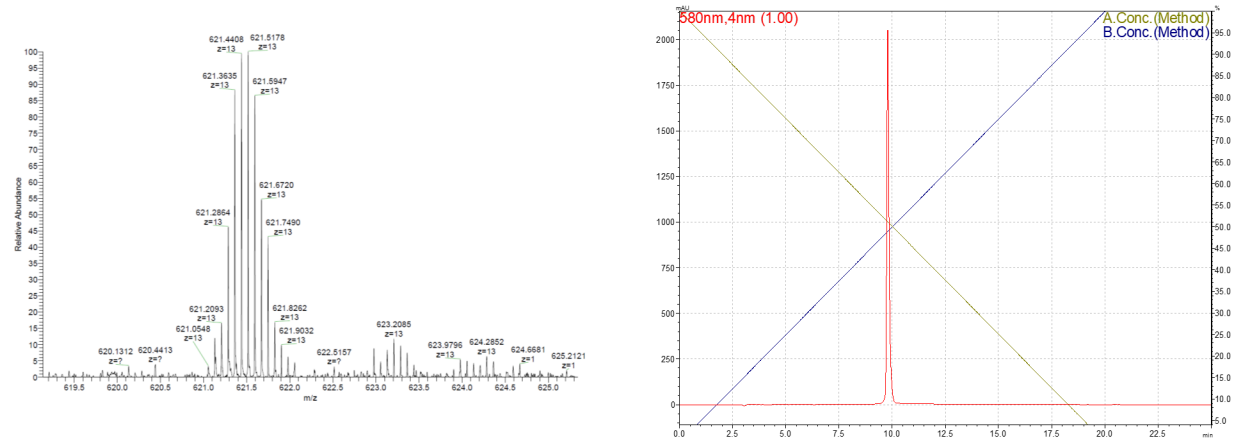

Figure S4. Analytical characterization of chromophore serial $\Delta 2$ ssDNA. Left: nanoelectrospray ionization mass spectrum. Right: high performance liquid chromatogram.

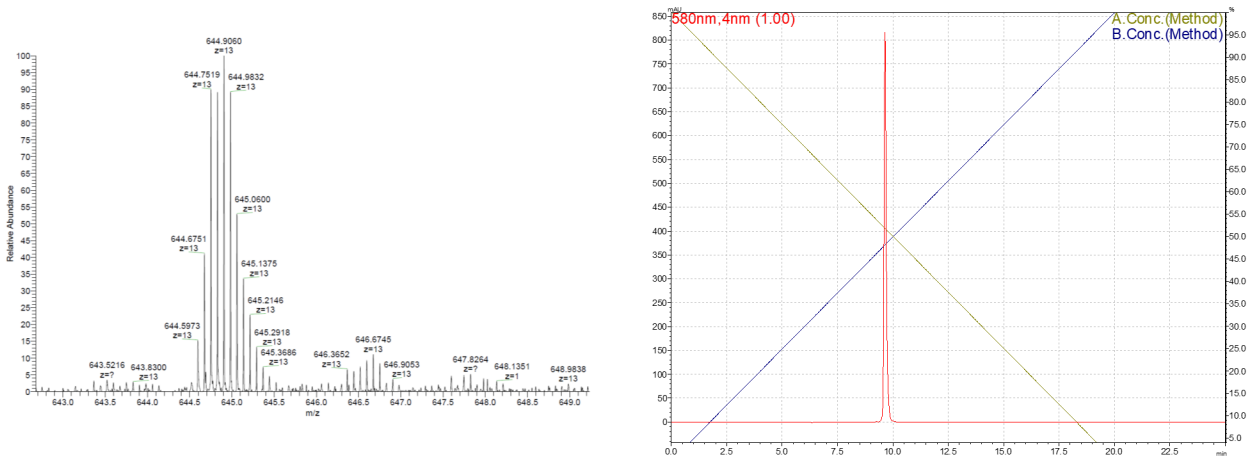

Figure S5. Analytical characterization of chromophore serial $\Delta 3$ ssDNA. Left: nanoelectrospray ionization mass spectrum. Right: high performance liquid chromatogram.

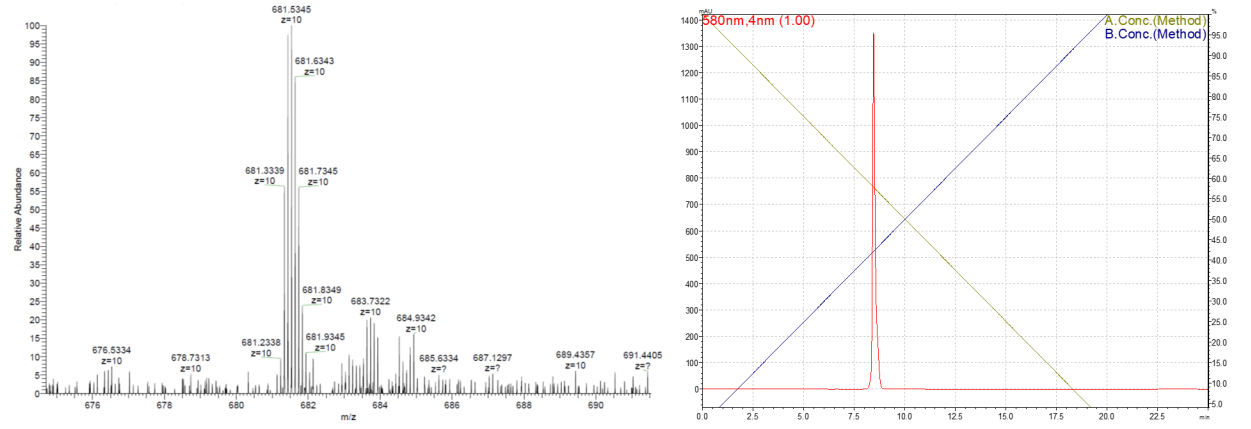

Figure S6. Analytical characterization of chromophore parallel $\Delta 0$ ssDNA A. Left: nanoelectrospray ionization mass spectrum. Right: high performance liquid chromatogram.

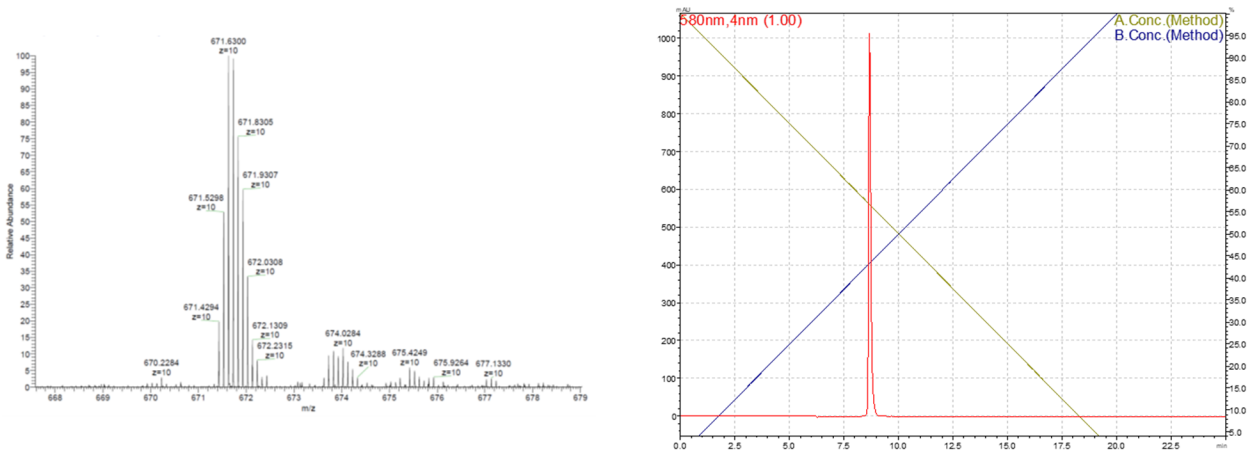

Figure S7. Analytical characterization of chromophore parallel $\Delta 0$ ssDNA B. Left: nanoelectrospray ionization mass spectrum. Right: high performance liquid chromatogram.

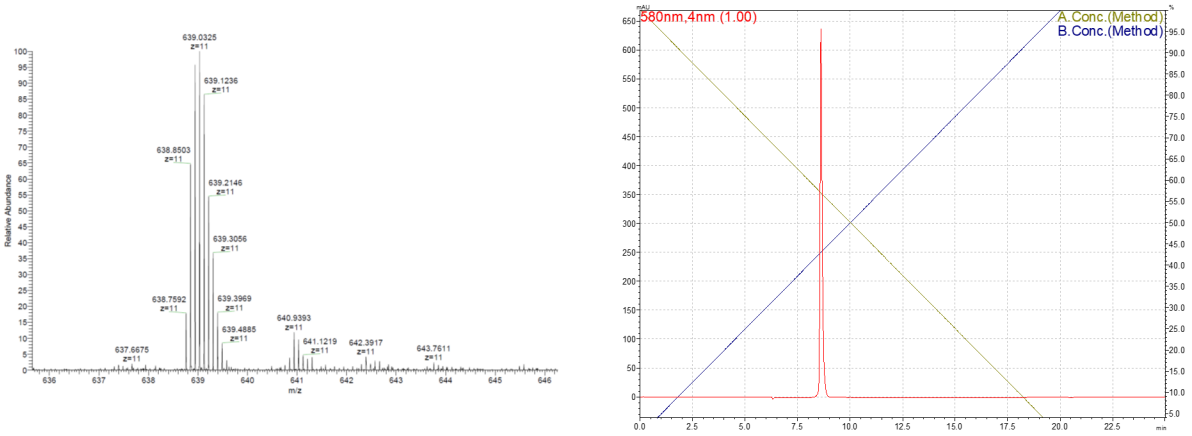

Figure S8. Analytical characterization of chromophore parallel $\Delta 1$ ssDNA A. Left: nanoelectrospray ionization mass spectrum. Right: high performance liquid chromatogram.

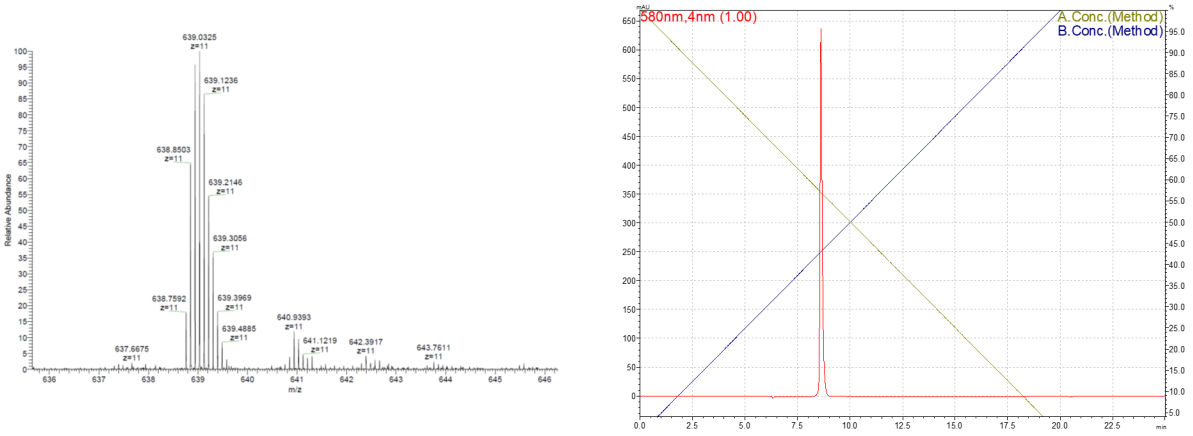

Figure S9. Analytical characterization of chromophore parallel $\Delta 1$ ssDNA B. Left: nanoelectrospray ionization mass spectrum. Right: high performance liquid chromatogram.

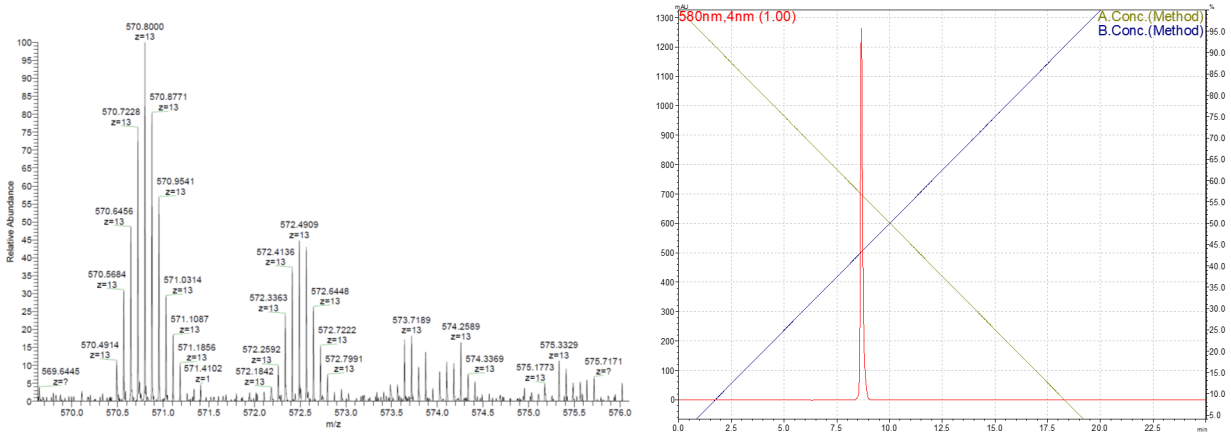

Figure S10. Analytical characterization of chromophore parallel $\Delta 2$ ssDNA A. Left: nanoelectrospray ionization mass spectrum. Right: high performance liquid chromatogram.

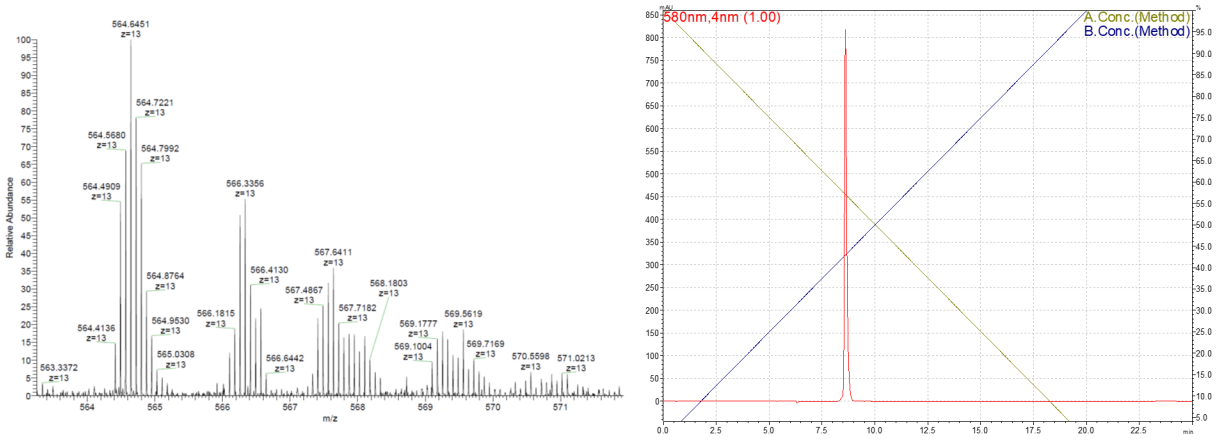

Figure S11. Analytical characterization of chromophore parallel $\Delta 2$ ssDNA B. Left: nanoelectrospray ionization mass spectrum. Right: high performance liquid chromatogram.

S1.3 Native polyacrylamide gel electrophoresis analysis

Hybridized DNA strands of squaraine-DNA constructs were analyzed using native polyacrylamide gel electrophoresis (PAGE). Using Bio-Rad Mini-PROTEAN® electrophoresis cells, squaraine-DNA duplexes (50 picomole per sample) were loaded into 12% PAGE gels that were supplemented with 1× tris(hydroxymethyl)aminomethane borate (TBE; Thermo Fisher; catalog number: 15581044) and 10 mM $MgCl_2$ and ran at 100 V for 30 minutes with 1× TBE as running buffer. Gels were subsequently immersed for 10 minutes in distilled water that contained 1× SYBR Gold nucleic acid stain (Thermo Fisher; catalog number: S11494). The stained gels were then imaged using a Typhoon FLA 7000 laser scanner (GE Healthcare).

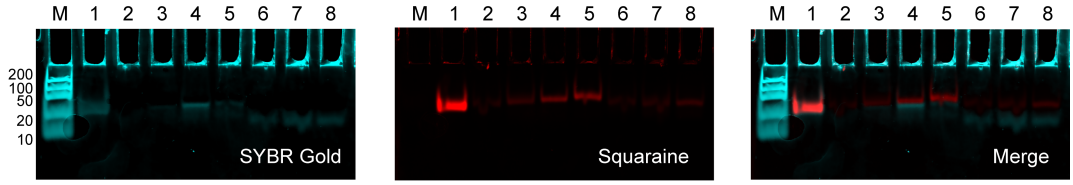

Figure S12. Native PAGE analysis of squaraine-DNA duplexes. **M**: FastRuler Ultra Low Range DNA ladder (Thermo Fisher; catalog number: SM1233), **1**: Squaraine monomer ssDNA + Canonical strand 1 ssDNA, **2**: Serial $\Delta 0$ ssDNA + Canonical strand 2 ssDNA, **3**: Serial $\Delta 1$ ssDNA + Canonical strand 3 ssDNA, **4**: Serial $\Delta 2$ ssDNA + Canonical strand 4 ssDNA, **5**: Serial $\Delta 3$ ssDNA + Canonical strand 5 ssDNA, **6**: Parallel $\Delta 0$ ssDNA A+ Parallel $\Delta 0$ ssDNA B, **7**: Parallel $\Delta 1$ ssDNA A + Parallel $\Delta 1$ ssDNA B, **8**: Parallel $\Delta 2$ ssDNA A + Parallel $\Delta 2$ ssDNA B.

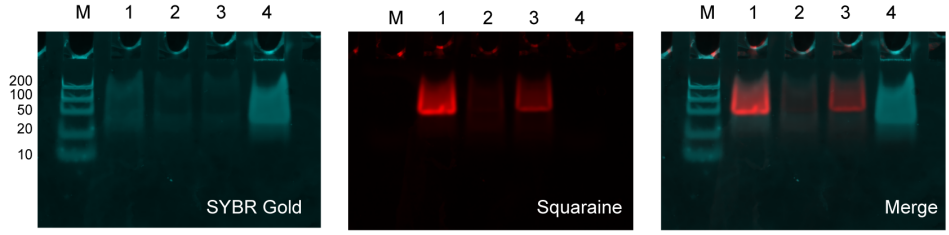

Figure S13. Native PAGE analysis of squaraine-DNA stem-loop constructs. **M**: FastRuler Ultra Low Range DNA ladder (Thermo Fisher; catalog number: SM1233), **1**: Squaraine monomer ssDNA + Stem loop-3 (Stem loop-3 monomer), **2**: Serial $\Delta 0$ ssDNA + Stem loop-3 (Stem loop-3 $\Delta 0$), **3**: Serial $\Delta 3$ ssDNA + Stem loop-3 (Stem loop-3 $\Delta 3$), **4**: Stem loop-3 control.

S1.4 DNA thermal denaturation

DNA thermal denaturation experiments were performed using an Agilent Cary 3500 UV-Vis spectrophotometer. A volume of 100 μl of sample was added in each cuvette then an additional 100 μl of mineral oil was carefully added to the sample without mixing to reduce evaporation. Samples were heated from 25°C to 90°C at a rate of 1 °C min^{-1}. Absorbance at 260 nm were measured at 1°C intervals.

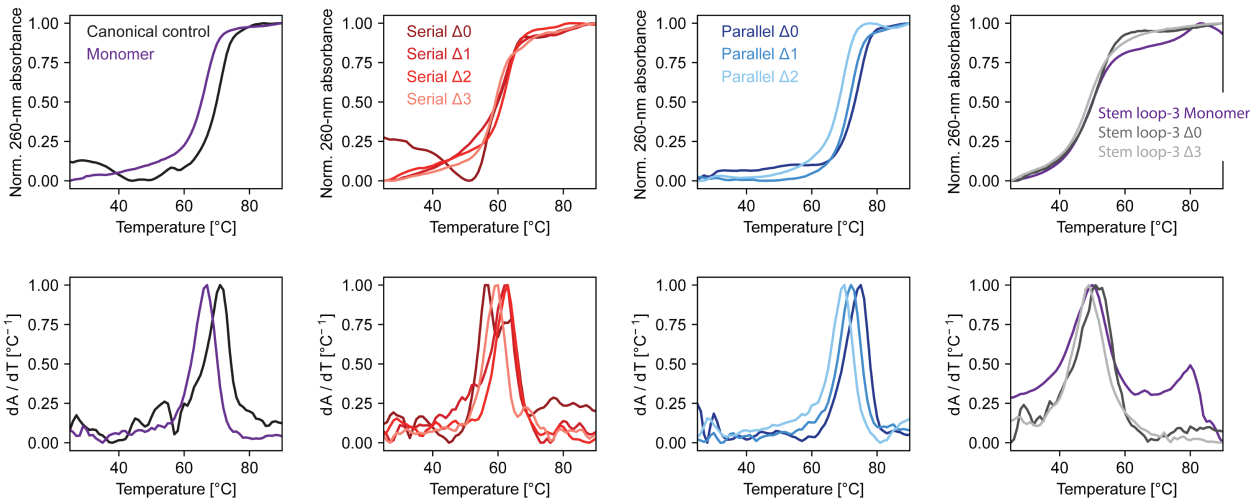

Figure S14. DNA thermal denaturation curves. Thermal denaturation curves of squaraine-dsDNA constructs (top) and corresponding first-derivative plots (bottom). [DNA] = 1.0 μM in 1× PBS. Stem loop monomer: Squaraine monomer ssDNA + Stem loop-3.

S1.5 Quantum yield measurements

Because the onset of the fluorescence spectra of cresyl violet is less than 600 nm, the full spectra of cresyl violet was extrapolated by first taking the fluorescence intensity ratio of the emission peak for cresyl violet (λ_{ems} = 625 nm) when excited at λ_{exc} = 590 nm ($I_{590,625}$) and 540 nm ($I_{540,625}$) then multiplying the calculated ratio to the fluorescence spectra of cresyl violet when excited at 540 nm ($I_{540,cv}$) to obtain the extrapolated full spectra of cresyl violet ($I_{ext,cv}$):

$$\int_{800\ \mathrm{nm}}^{550\ \mathrm{nm}} I_{\mathrm{ext,cv}}\mathrm{d}\lambda = \frac{I_{590,625}}{I_{540,625}} \int_{800\ \mathrm{nm}}^{550\ \mathrm{nm}} I_{540,\mathrm{cv}}\mathrm{d}\lambda \tag{S1}$$

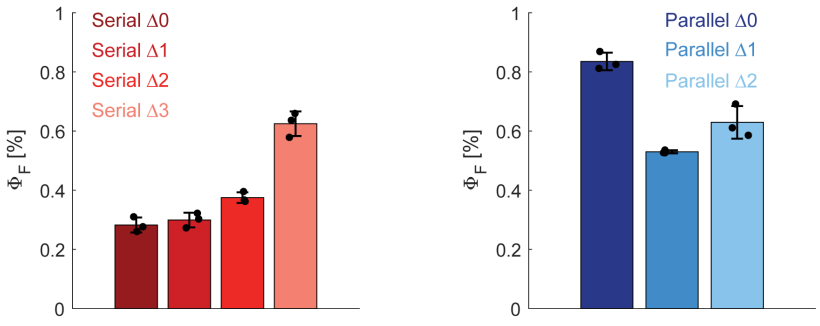

Figure S15. Quantum yields of serial and parallel squaraine dimer DNA duplex constructs. The quantum yields of squaraine dimer constructs were measured at a concentration of 0.5 μM in 1× PBS and using cresyl violet as reference. Bar height indicates the average of three independent replicates. Error bars denote the standard deviation of three independent measurements.

S2 Time-resolved emission spectroscopy

S2.1 Time-resolved single-photon counting experimental set-up

A pulsed excitation scheme was used to determine the ensemble lifetime through single-photon detection. Pump pulses were generated using an 80 MHz Ti:Sapphire laser source (Spectra Physics Mai Tai) and passed through a photonic crystal fiber (NKT photonics FemtoWhite 800) to generate a broadband continuum. The excitation wavelength was selected for using band pass filters. The excitation was set to 580 nm (10 pJ/pulse), while the emission was set to 635 nm. An avalanche photodiode was used to detect single-photons (Micro Photon Devices) in conjunction with a time-correlation module (Picoquant, PicoHarp 300). Histogrammed photon arrival times were then used to report on the excited state lifetime. Lifetime fits were achieved with fitting to a biexpoential decay convolved with the experimentally-measured 60-80 ps FWHM instrument response function (IRF):

$$I(t) = A_0 + \mathrm{IRF} \otimes \sum_{i=1}^{2} A_i \exp\left(-t/\tau_i\right) \tag{S2}$$

S2.2 DNA-squaraine construct emission lifetimes

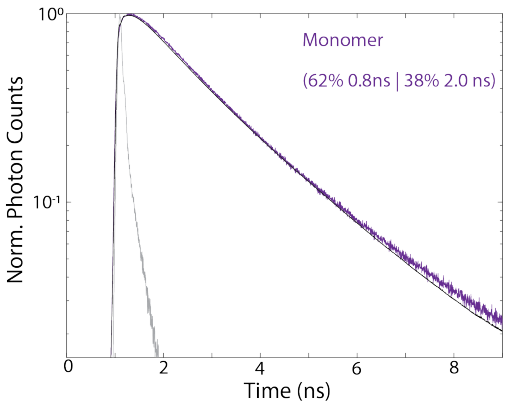

Figure S16. Monomer emission lifetime. Monomer emission fit to a biexponential decay convolved with the instrument response function (shown in gray), yielding an average lifetime of 1.3 ns.

S3 Theoretical model

An initial approach to describe the excitonic interactions in squaraine dimers scaffolded in DNA is by employing the Frenkel-Holstein model, which includes the electronic Hamiltonian of the system as well as the effect of the coupling to the phonon bath:

$$H_{\mathrm{FE}} = H_{\mathrm{el}} + H_{\mathrm{vib}} \tag{S3}$$

$$H_{\mathrm{el}} = \sum_{n}^{2} H_{\mathrm{el}}^{n} + \sum_{m,n}^{2} V_{\mathrm{excitonic}} |m\rangle\langle n| \tag{S4}$$

where H_{el}^{n} is the electronic Hamiltonian describing monomer n, while $V_{\mathrm{excitonic}}$ describes the long-range excitonic interaction between an exciton localized in monomers m and n. Using time-dependent density functional theory (TDDFT) or configuration interaction singles (CIS) with the Tamn-Dancoff approximation (TDA), we can write the coupling $V_{\mathrm{excitonic}}$ in terms of two-electron integrals of occupied and virtual orbitals,

$$V_{\mathrm{excitonic}} = \sum_{i,a,j,b} c_{i,a}^{(1)} c_{j,b}^{(2)} [2(\psi_i^{(1)}\psi_a^{(1)}|\psi_j^{(2)}\psi_b^{(2)}) - (\psi_i^{(1)}\psi_j^{(2)}|\psi_a^{(2)}\psi_b^{(1)})]. \tag{S5}$$

where $\psi_i^{(1)}$ represents the orbital i in monomer 1, and $c_{i,a}^{(1)}$ is the CIS coefficient describing the excitation of a single electron from occupied MO i to virtual MO a. The first term in Equation S5 is referred as a Coulomb integral, $(ia|jb) = \int dr_1 dr_2 \psi_i^*(r_1)\psi_a(r_1) r_{12}^{-1} \psi_j^*(r_2)\psi_b(r_2)$, while $(ij|ab)$ is an exchange integral and is often negligible unless molecules exhibit a significant spatial overlap. Although some of the dimer geometries in this study exhibit some molecular orbital overlap, the calculated values for the exchange integral were two to three orders-of-magnitude lower than the Coulomb integral and thus can be ignored.

Equation S5 can be further simplified by writing the coupling in terms of interactions between transition charge monopoles, or individual charges located at each atom, [1, 2]

$$V_{\text{excitonic}} \approx \sum_{k,l} \frac{q_k^{(1)} q_l^{(2)}}{r_k^{(1)} - r_l^{(2)}}, \tag{S6}$$

where $q_k^{(1)}$ is a transition charge located on the k^{th} atom of molecule 1, and $r_k^{(1)}$ is the position of that atom. We found that the expression in Equation S6 considerably underestimated the coupling $V_{\text{excitonic}}$ (Figure S17), while the computational cost for the expression in Equation S5 was comparable. Thus, Equation S5 was employed in this study.

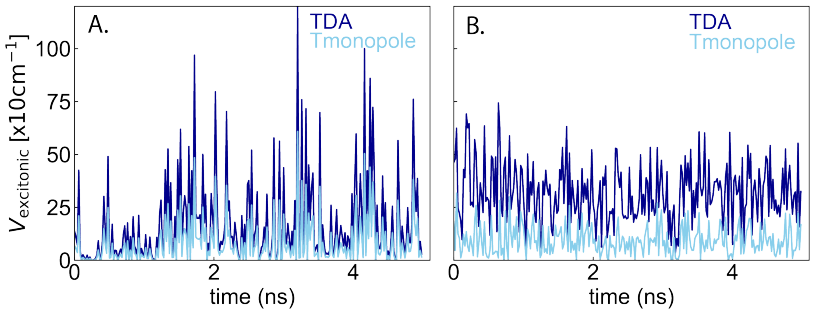

Figure S17. Calculating the excitonic coupling. Comparison of $V_{\text{excitonic}}$ calculated for the serial (A) and parallel (B) dimers employing Equation S5 vs Equation S6.

However, to fully describe the electronic properties of squaraine dimers, we need to quantify the effect of charge transfer (CT) short-term interactions as well. When the intramolecular distance of the dimer is small and the Frenkel and CT energetic bands are well separated, the electron and hole can be transferred from one monomer to the other through a virtual CT state. This interaction gives rise to a short-range electronic coupling that can be described in terms of electron and hole integrals, t_e and t_h,

$$V_{\text{CT}} \approx -2\frac{t_e t_h}{(\varepsilon_{\text{CT}} - \varepsilon_{\text{FE}})}, \tag{S7}$$

where ε_{CT} and ε_{FE} are the energies corresponding to the CT state and the Frenkel exciton, respectively. The energy of the CT state can also be separated in terms of the energy of the unbound CT pair, $\varepsilon_{\text{CT}}^{\text{unb}}$ and its Coulombic binding energy, $U_{\text{CT}} = e^2/4\pi\epsilon_0\epsilon_R|r|$,

$$\varepsilon_{\text{CT}} = \varepsilon_{\text{CT}}^{\text{unb}} - U_{\text{CT}}. \tag{S8}$$

where ϵ_0 and ϵ_R are the dielectric constant of vacuum and water, respectively. The term $U = \varepsilon_{\text{CT}}^{\text{unb}} - \varepsilon_{\text{FE}}$ can be interpreted as the binding energy of the local excitation and has little impact in the overall coupling V_{CT}. Computation of the binding energy, U, is expensive and it is very unlikely to affect the statistical distribution of the coupling. Therefore, U was taken as a constant and set to 0.7 eV [3]. On the other hand, the electron and hole integrals are defined as,

$$\begin{aligned} t_e &= \langle L^{(1)}|h|L^{(2)}\rangle \\ t_h &= -\langle H^{(1)}|h|H^{(2)}\rangle, \end{aligned} \tag{S9}$$

where $L^{(1)}$ and $H^{(1)}$ are the LUMO and HOMO of molecule 1, respectively, and h is the 1-electron Hamiltonian. Now, having defined both $V_{\text{excitonic}}$ and V_{CT} we define the total coupling resulting from interfering long and short-range effects as,

$$V_{\text{total}} = V_{\text{excitonic}} + V_{\text{CT}}. \tag{S10}$$

The excitonic coupling was calculated with the TDDFT/TDA method applied to the monomers separately, with the 2-electron integrals defined by Equation S5. While DFT on the isolated monomers was employed to calculate the electron and hole integrals according to Equation S9.

S4 Molecular dynamics simulations of serial and parallel squaraine constructs

S4.1 Squaraine force field generation

A.

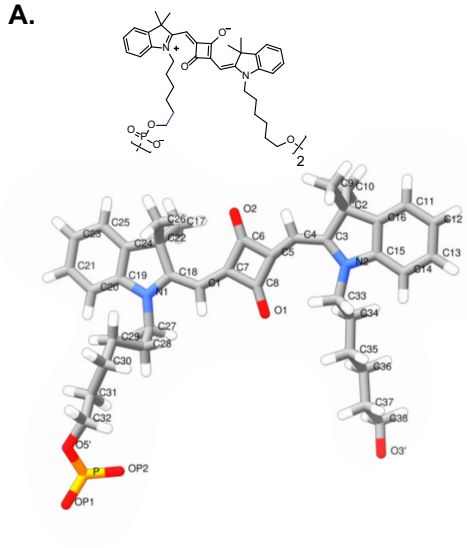

B.

Atom	Type	Charge	Atom	Type	Charge	Atom	Type	Charge
N1	n2	-0.1737	H13	hc	0.0499	C31	c3	-0.1104
N2	n2	-0.1737	H14	hc	0.0499	H31	hc	0.0435
C1	c2	-0.3091	H15	hc	0.0499	H32	hc	0.0435
H1	ha	0.1485	C18	c2	0.3446	C32	c3	0.1909
C2	c3	-0.0520	C19	ca	0.0038	H33	h1	0.0280
C3	c2	0.3446	C20	ca	-0.1475	H34	h1	0.0280
C4	c2	-0.3091	H16	ha	0.1555	C33	c3	0.0368
H2	ha	0.1485	C21	ca	-0.1015	H35	h1	0.0612
C5	c2	-0.1614	H17	ha	0.1360	H36	h1	0.0612
C6	c2	0.5245	C22	c3	-0.0520	C34	c3	-0.1029
C7	c2	-0.1614	C23	ca	-0.1615	H37	hc	0.0657
C8	c2	0.5245	H18	ha	0.1285	H38	hc	0.0657
C9	c3	-0.0834	C24	ca	-0.1338	C35	c3	-0.0774
H3	hc	0.0499	C25	ca	-0.0845	H39	hc	0.0347
H4	hc	0.0499	H19	ha	0.1355	H40	hc	0.0347
H5	hc	0.0499	C26	c3	-0.0834	C36	c3	-0.0759
C10	c3	-0.0834	H20	hc	0.0499	H41	hc	0.0380
H6	hc	0.0499	H21	hc	0.0499	H42	hc	0.0380
H7	hc	0.0499	H22	hc	0.0499	C37	c3	-0.1104
H8	hc	0.0499	C27	c3	0.0368	H43	hc	0.0435
C11	ca	-0.0845	H23	h1	0.0612	H44	hc	0.0435
H9	ha	0.1355	H24	h1	0.0612	O3'	OS	-0.5767
C12	ca	-0.1615	C28	c3	-0.1029	O1	O2	-0.5961
H10	ha	0.1285	H25	hc	0.0657	O2	O2	-0.5961
C13	ca	-0.1015	H26	hc	0.0657	OP1	O2	-0.8233
H11	ha	0.1360	C29	c3	-0.0774	P	P	1.4218
C14	ca	-0.1475	H27	hc	0.0347	O5'	OS	-0.5767
H12	ha	0.1555	H28	hc	0.0347	C38	c3	0.1909
C15	ca	0.0038	C30	c3	-0.0759	H45	h1	0.0280
C16	ca	-0.1338	H29	hc	0.0380	H46	h1	0.0280
C17	c3	-0.0834	H30	hc	0.0380	OP2	O2	-0.8233

Figure S18. Generation of a Force Field for the molecular dynamics simulations. (A) Molecular and atomic coordinates for squaraine with hexyl linker. Heavy atom names are labeled. (B) Modified force field for squaraine. The table lists atom types and charges following the AMBER GAFF2.

Prior to the all-atom MD simulations, a force field (FF) was generated for the squaraine molecule and its hexyl linkers. The modified squaraine molecule was modeled using the Avogadro molecular editor (version 1.2.0) [4], and the geometry was optimized with the restricted Hartree-Fock (RHF) method and the 6-31G(d) basis set [5]. The atomic point charges were generated with the AM1-BCC method [6] included in the Antechamber package [7]. The charges of the phosphate linkage were chosen to resemble those of DNA nucleotides and the generalized Amber force field (GAFF) [8] was employed for all FF terms (Figure S18).

S4.2 All-atom Molecular Dynamics simulations

The variation of the intramolecular distance for both types of dimers is shown in Figure S19C, as a function of time, while the variation of $V_{\text{excitonic}}/V_{\text{CT}}$ is shown in Figure S19D. Given the change in intramolecular distance remains fairly stable thorough the simulation, the variation in coupling likely comes from differences in the relative orientation of the monomers.

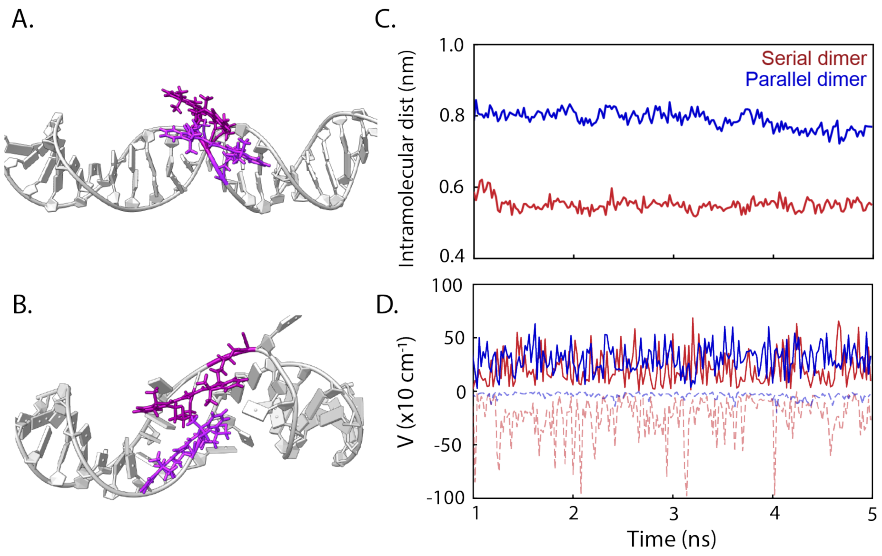

Figure S19. Molecular dynamics simulation results for the parallel and serial $\Delta 0$ duplexes. Initial coordinates employed for the (A) serial and (B) parallel $\Delta 0$ duplex dimers. (C) Time evolution of the intramolecular distance for both dimers for the 5 ns duration of the production MD. (D) Time evolution of the excitonic (solid line) and CT (dashed line) couplings.

S4.3 Excited state calculations on squaraine dimers

The coordinates of each squaraine molecule were extracted from the MD trajectories every 20 ps with the MDAnalysis package [9] (250 frames in total). Then, the phosphate groups in the squaraine linkers were replaced with hydrogen atoms, and DFT was performed with a 6-31G level of theory and implicit COSMO solvation using PySCF [10]. These results were employed to calculate V_{CT} as described in Section S3, while TDDFT/TDA was performed with a B3LYP functional to calculate $V_{\mathrm{excitonic}}$. Other excited state properties needed to reproduce optical properties for squaraine were also calculated, namely, the excitation energy, transition dipole moment, and the oscillator strength.

S4.4 Choice of initial coordinates for the parallel dimer

Given the timescale required for DNA equilibration is significantly longer than the timescale for the detection of CT effects, the initial state of the DNA-squaraine construct was carefully selected so that experimental results could be reproduced within a reasonable computational cost.

When constructing the initial configuration of the parallel $\Delta 0$ dimer, the most straightforward approach for placing the two molecules parallel to each other is by placing the monomers pointing on opposite sides of the DNA chain (Figure S20A). This is because the large size of squaraine—with a diameter of $\sim$ 15Å—leads to prohibitive steric constrains if placed closer to the center of the duplex. This configuration, however, places the molecules at a distance greater than $\sim$ 20Å from each other, i.e., the diameter of DNA, rendering the distance-dependent excitonic coupling to almost zero (Figure S20D and E). To reproduce the results observed experimentally we explore other possible configurations were monomers were initially placed closer to each other. For example, one possible stable arrangement will have the molecules located inside of the DNA major grooves (Figure S20B). As seen in Figure S20D, this placement only decreases the intramolecular distance of the dimer to the diameter of DNA and will lead to negligible coupling as well.

Based on the previous arguments, the only reasonable strategy to construct the parallel $\Delta 0$ duplex such that the observed coupling is reproduced is by placing the dimer inside of the DNA duplex. However, given the large size of squaraine, placing one or both monomers will lead to destabilization of the DNA double-chain structure, as some of the hydrogen bonds between complementary bases would have to be separated to make space for the squaraine molecule. Following this strategy, both base pairs adjacent to the dimer were pushed in the opposite direction of the center of the duplex, and the dimer was arranged inside the DNA structure with a significantly smaller intramolecular distance between monomers (Figure S20B). The simulated trajectory employing the latter as an initial structure re-

sulted in monomer-to-monomer distances very close to those in the serial dimer, and $V_{\text{excitonic}}$ close to that observed experimentally (Figures S20D and E).

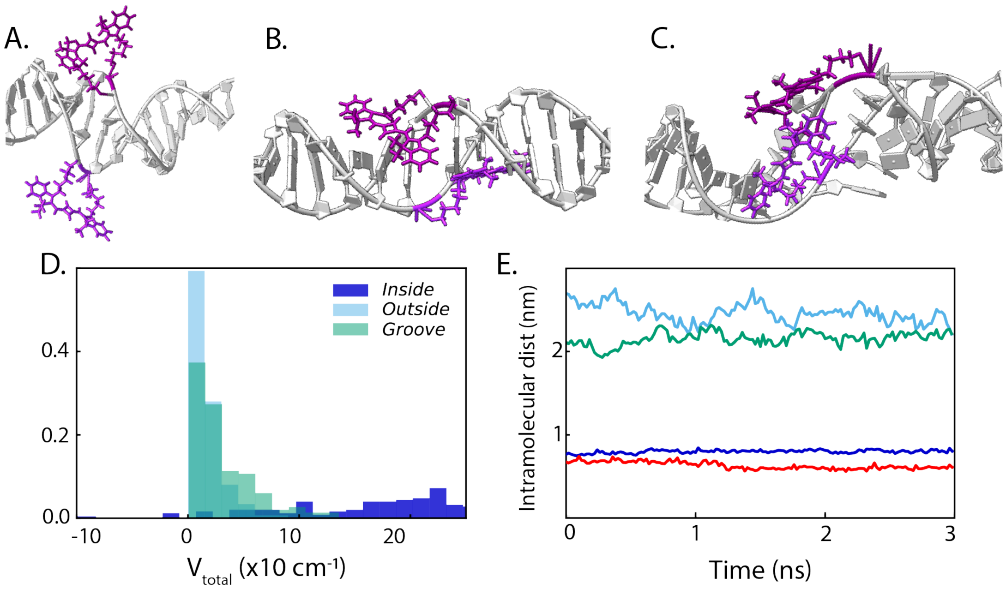

Figure S20. Finding the parallel $\Delta 0$ duplex configuration more closely resembling the experiment. Snapshots from the MD trajectories for (A) the dimer configuration on opposite directions across the duplex, (B) the dimer configuration on DNA major grooves and (C) the DNA configuration with the dimer placed inside the duplex, as described in the text. (D) Histogram with the total coupling for the 3 dimer configurations. (E) Intradimer distance for the 3 configurations and the serial configuration(red).

S5 Umbrella sampling calculation on the isolated dimer

Nevertheless, the described rearrangement of the DNA duplex will only occur if the intermolecular strength between the squaraine monomer is large enough to promote the breakage of the hydrogen bonds between the base pairs. Specifically, the stabilization induced by the aggregation of squaraine needs to be larger that the destabilization resulting from the separation of a few complementary base pairs. We attempt to test the feasibility of the initial configuration chosen for the parallel $\Delta 0$ dimer by comparing the intermolecular forces of squaraine aggregation, with the strength of DNA base pairs. If these two magnitudes are comparable, we believe that the proposed structure (Figure S20A) is energetically justified. With this in mind, umbrella sampling (US) calculations were employed on the isolated squaraine dimer to determine the potential energy surface (PES) associated with the dimer disaggregation.

First, the coordinates of the squaraine dimer were extracted from the parallel $\Delta 0$ duplex initial structure in Figure S19B, after MD minimization is performed. MD simulations were carried out using the Amber18 software and the same FF from Section S4.1, with TI3P explicit solvation of the isolated dimer. Following the protocol outlined in Ref. [11], a restrained minimization of the initial structure was performed for 5000 steps each, followed by 5000 steps of unrestrained minimization for the entire system, both with a 12Å cutoff. This was followed by a NVT heating of the solvent to 300 K, for 20 ps. Then, a NPT equilibration of the entire system was carried out by gradually reducing the imposed harmonic constrain on the system on 4 steps, with 30 ps each: from 50 to 10, 5 and 0 kcal mol^{-1}Å^{-2}. Finally, the US method was employed for the free energy calculation of the final equilibrated structure [12]. To construct the potential mean field (PMF) for squaraine aggregation, the dimer was constrained on a biased potential across a range of intramolecular separations with a harmonic restrain of 100 kcal mol^{-1}Å^{-2}. Here, the intramolecular distance was defined as the separation between the C7 atoms on each squaraine molecule, identified as the closest to the center of mass of the molecule(see Figure S18A). A total of 90 windows were constructed by varying the center of the biased potential from 3 to 12Å, every 0.1Å. For each window, a 2000 step minimization, a 40 ps NPT equilibration and 100 ps NPT production were simulated, with biased coordinates recorded every 4 ps of the production run (a total of 2500 recorded per window). Then, the WHAM algorithm [13], as implemented by Alan Grossfield [14], was employed to

process the biased coordinates with a converged tolerance of 0.00001, and the free energy of aggregation was calculated form the obtained PMF (Figure 2C on the main text). The WHAM result was tested for accuracy by manually calculating the PMF from each of the biased distributions, for each window, confirming the convergence of the code.

As can be appreciated in Figure S20A, we note that the stability of the proposed process is too complex to be explained through a couple of interactions between nucleotides, as the placement of the dimer inside the duplex leads to a rearrangement of all surrounding nucleotide pairs, some becoming more stable than others, and the energetic interactions of the DNA-dye structure becomes more complicated as the entire system reaches equilibrium. However, we believe the presented comparison of the squaraine dimer stability with that for DNA base pairings provides a reasonable guide to the structural arrangement that the DNA-squaraine complex will adopt under the present experimental conditions.

S6 Prediction of the absorption spectra

The predicted absorption spectra can also be constructed based on the MD results. Based on an ensemble of dimer configurations generated from the resulting trajectories, we can define a Hamiltonian in the site basis describing the excitonic state,

$$H_i = \begin{pmatrix} \varepsilon_i^{(1)} & V_i \\ V_i & \varepsilon_i^{(2)} \end{pmatrix}, \tag{S11}$$

where $\varepsilon_i^{(1)}$ and $\varepsilon_i^{(2)}$ are the excited state energies for the two molecules, and V_i the electronic coupling of the dimer in the configuration i. Solving for the eigenstates of the Hamiltonian in Equation S11 we get the set of eigenstates,

$$\begin{aligned} \psi_i^{(A)} &= C_{1,i}^{(A)}\phi_i^{(1)} + C_{2,i}^{(A)}\phi_i^{(2)} \\ \psi_i^{(B)} &= C_{1,i}^{(B)}\phi_i^{(1)} + C_{2,i}^{(B)}\phi_i^{(2)}, \end{aligned} \tag{S12}$$

Similarly, we can define the oscillator strength in the eigenbasis as,

$$\begin{aligned} \mu_i^{(A)} &= C_{1,i}^{(A)}\mu_i^{(1)} + C_{2,i}^{(A)}\mu_i^{(2)} \\ \mu_i^{(B)} &= C_{1,i}^{(B)}\mu_i^{(1)} + C_{2,i}^{(B)}\mu_i^{(2)}, \end{aligned} \tag{S13}$$

with eigenvectors $\{C_{1,i}^{(A,B)}, C_{2,i}^{(A,B)}\}$ and eigenvalues $\lambda_i^{(A,B)}$. The absorption spectra $I(E)$ of the ensemble $i = 1, 2, ..., N$ can be defined as an histogram weighted by the oscillator strength,

$$I(E) \propto \sum_{i=1}^{N} \sum_{\alpha=A,B} \mu_i^{(\alpha)} \delta(\lambda_i^{\alpha} - E). \tag{S14}$$

The delta function $\delta(\lambda_i^{\alpha} - E)$ can also be replaced by a gaussian function resulting in the expression,

$$I(E) \propto \sum_{i=1}^{N} \sum_{\alpha=A,B} \mu_i^{(\alpha)} \exp[-(\lambda_i^{\alpha} - E)^2/2\sigma^2]. \tag{S15}$$

We constructed an ensemble with the data extracted from the MD simulations with $N = 750$ for the parallel $\Delta 0$ dimer and $N = 500$ for the serial, and calculated the oscillator strength $\mu_i^{(1,2)}$ and the excitation energies $\varepsilon_i^{(1,2)}$ as described in Section S4.3. To understand the effect of the CT coupling on the predicted absorption spectra, we used Equation S15 to calculate the spectra both using $V_{\mathrm{excitonic}}$ alone without CT, i.e., taking $V_{\mathrm{excitonic}}$ as V_i in Equation S11, and with V_{total} as V_i to include CT. Figure S21 shows the spectra calculated using Equation S15 and the excitonic coupling, while the results using the total coupling V_{total} are presented in dashed lines t. As expected, the CT increases the vibronic band ratio 0-0/0-1. The monomer peak is approximated from the resulting dynamics on

the DNA-dye structure showed in Figure S20B, where the intramolecular distance is > 24Å and the dimer is seen to have a monomer-like behavior.

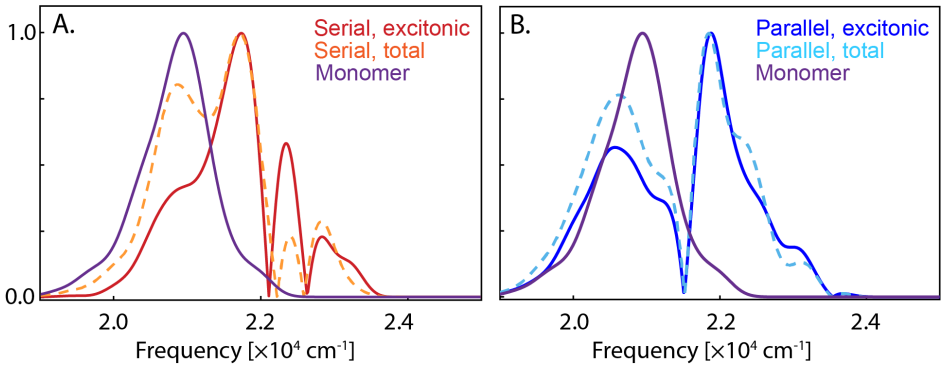

Figure S21. Absorption spectra as calculated from the MD trajectories. Predicted spectra for (A) the serial and (B) the parallel $\Delta 0$ dimer. The dashed line indicates the spectra calculated adding the effect of the CT coupling, as described in the text. The width of the absorption peaks is given by $\sigma = 350$ cm^{-1} in all cases.

S7 Femtosecond transient absorption spectroscopy

S7.1 Experimental set-up

The broadband transient absorption set-up is described elsewhere [15, 16]. Wavelength dependent dispersion was corrected for post-processing with a dye standard. The pump and probe spectra are shown in Figure S22 below, along with the cross correlation between the pump and probe measured through second harmonic generation.

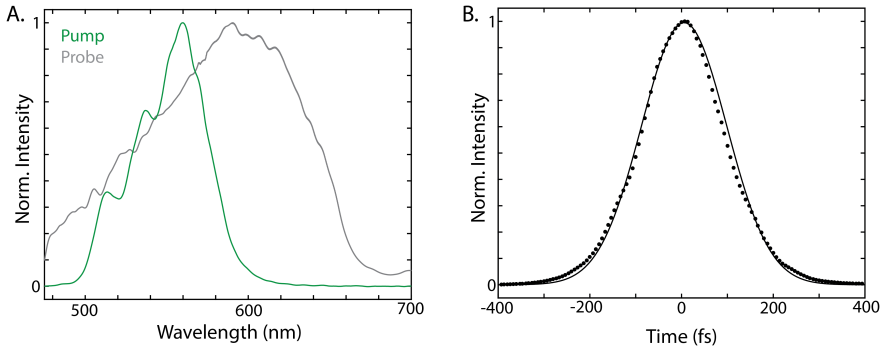

Figure S22. Characterization of femtosecond pulses. (A) Spectra profile of pump (derived from frequency resolved optical gating experiment) and probe pulses used for the femtosecond transient absorption experiments. (B) Cross correlation between pump and probe pulses yields a 200 fs FWHM (additional length arising from dispersion and mismatch between center frequency and blaze wavelength).

S7.2 Transient absorption spectra and timescale fits for monomer species

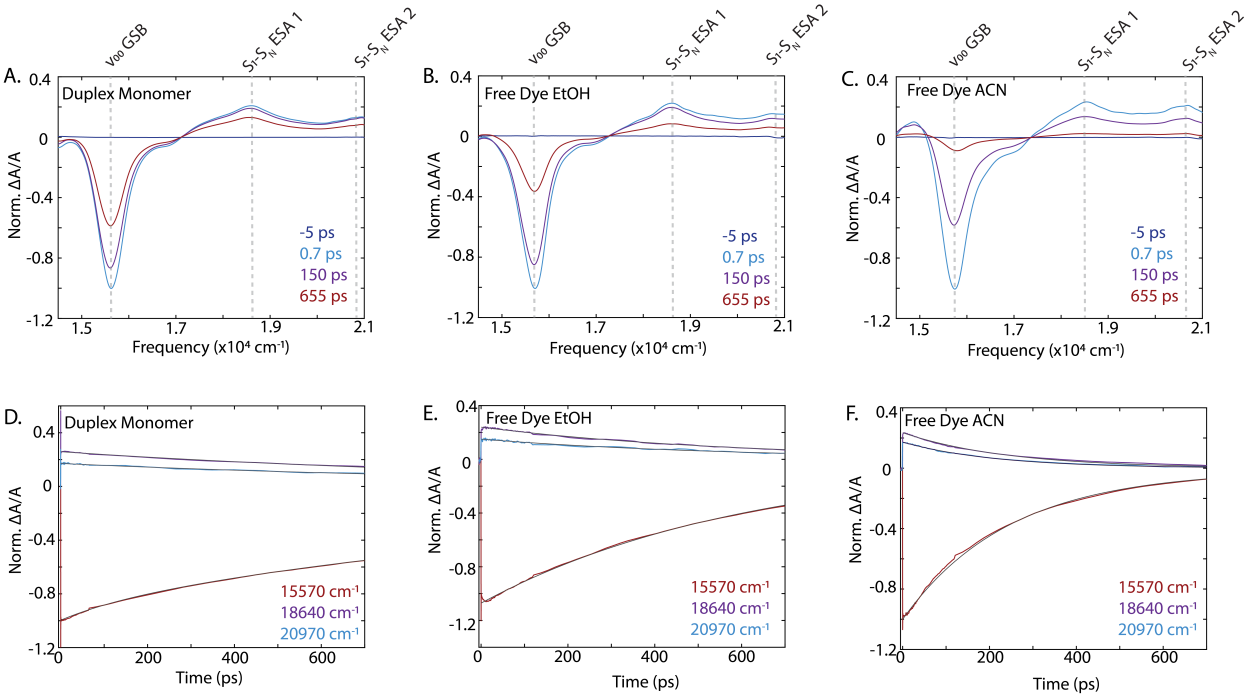

Figure S23. Monomer squaraine transient absorption. Transient absorption (ΔA/A) spectra for monomeric (A) DNA duplex bound squaraine, (B) squaraine free dye in ethanol, and (C) squaraine free dye in acetonitrile. Time domain transient absorption traces in for ground state bleach and excited state absorption bands for monomeric (D) DNA duplex bound squaraine, (E) squaraine free dye in ethanol, and (F) squaraine free dye in acetonitrile.

Table S3. Time domain fit parameters for monomer transient absorption experiments.

	A_1	τ_1	A_2	τ_2
DNA duplex (ν_{00} GSB)	0.1	140 ps	0.9	1.4 ns
DNA duplex (S_1-S_N ESA 1)	1.0	1.1 ns	-	-
DNA duplex (S_1-S_N ESA 2)	1.0	610 ps	-	-
Free dye in ethanol (ν_{00} GSB)	1.0	610 ps	-	-
Free dye in ethanol (S_1-S_N ESA 1)	1.0	580 ps	-	-
Free dye in ethanol (S_1-S_N ESA 2)	1.0	580 ps	-	-
Free dye in acetonitrile (ν_{00} GSB)	1.0	240 ps	-	-
Free dye in acetonitrile (S_1-S_N ESA 1)	1.0	240 ps	-	-
Free dye in acetonitrile (S_1-S_N ESA 2)	1.0	220 ps	-	-

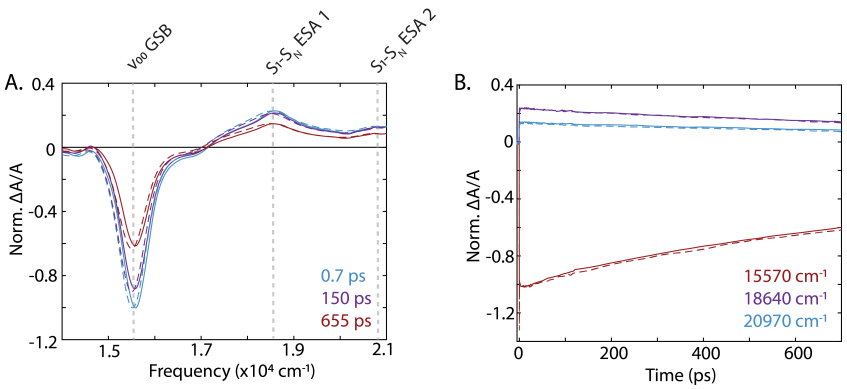

Figure S24. Squaraine stem loop-3 monomer construct transient absorption. Transient absorption (A) spectra and (B) time traces for monomeric squaraine in DNA stem-loop motif. Solid lines correspond to 100% aqueous conditions, dashed lines correspond to 70% aqueous and 30% DMF conditions.

Table S4. Time domain fit parameters for stem-loop monomer construct transient absorption experiments.

	A_1	τ_1	A_2	τ_2
Stem loop-3 in 0% DMF (ν_{00} GSB)	0.1	150 ps	0.9	1.6 ns
Stem loop-3 in 0% DMF (S_1-S_N ESA 1)	1.0	1.3 ns	-	-
Stem loop-3 in 0% DMF (S_1-S_N ESA 2)	1.0	1.3 ns	-	-
Stem loop-3 in 30% DMF (ν_{00} GSB)	0.1	140 ps	0.9	1.5 ns
Stem loop-3 in 30% DMF (S_1-S_N ESA 1)	1.0	1.3 ns	-	-
Stem loop-3 in 30% DMF (S_1-S_N ESA 2)	1.0	1.2 ns	-	-

S7.3 Supplemental transient absorption spectra and timescale fits for stem loop-3 constructs

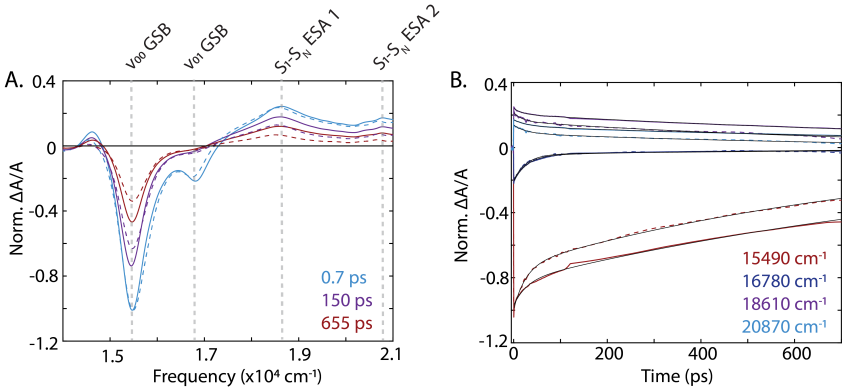

Figure S25. Stem loop-3 Δ3 dimer transient absorption. Transient absorption (A) spectra and (B) time traces for the stem loop-3 Δ3 construct. Solid lines correspond to 100% aqueous conditions, dashed lines correspond to 70% aqueous and 30% DMF conditions.

Table S5. Time domain fit parameters for stem-loop Δ3 dimer transient absorption experiments.

	A_1	τ_1	A_2	τ_2	A_3	τ_3
Stem loop-3 Δ3 in 0% DMF (ν_{00} GSB)	0.15	30 ps	0.85	1.1 ns	-	-
Stem loop-3 Δ3 in 0% DMF (ν_{01} GSB)	0.76	30 ps	0.24	680 ps	-	-
Stem loop-3 Δ3 in 0% DMF (S_1-S_N ESA 1)	0.12	12 ps	0.08	110 ps	0.80	1.3 ns
Stem loop-3 Δ3 in 0% DMF (S_1-S_N ESA 2)	0.24	30 ps	0.76	1.2 ns -	-	
Stem loop-3 Δ3 in 30% DMF (ν_{00} GSB)	0.27	30 ps	0.73	820 ps	-	-
Stem loop-3 Δ3 in 30% DMF (ν_{01} GSB)	0.80	30 ps	0.20	900 ps	-	-
Stem loop-3 Δ3 in 30% DMF (S_1-S_N ESA 1)	0.22	14 ps	0.34	380 ps	0.43	1.3 ns
Stem loop-3 Δ3 in 30% DMF (S_1-S_N ESA 2)	0.35	30 ps	0.65	700 ps -	-	

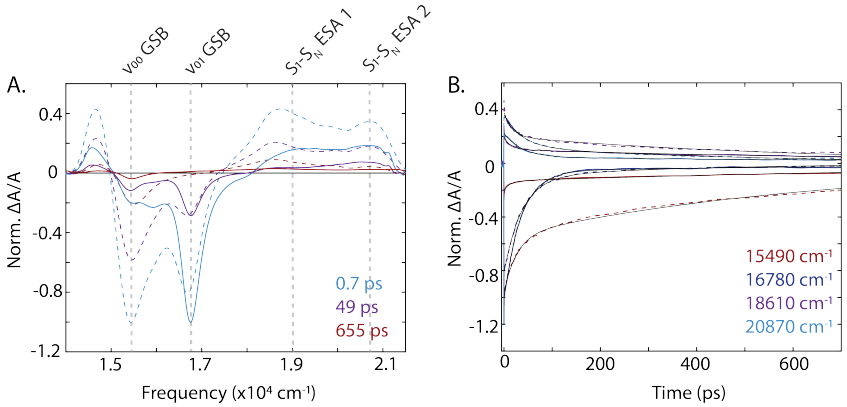

Figure S26. Stem loop-3 Δ0 dimer transient absorption. Transient absorption (A) spectra and (B) time traces for stem loop-3 Δ0 construct. Solid lines correspond to 100% aqueous conditions, dashed lines correspond to 70% aqueous and 30% DMF conditions.

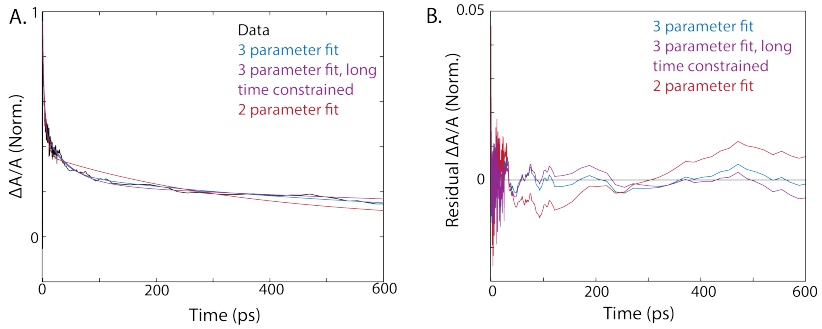

Figure S27. Transient absorption fit kinetics for stem loop-3 Δ0 construct ESA 1 band. (A) Two and three component fits overlaid with data (B) residual of two and three component fits.

Table S6. Time domain fit parameters for stem-loop Δ0 construct transient absorption experiments. (* indicates rise time)

	A_1	τ_1	A_2	τ_2	A_3	τ_3
Stem loop-3 Δ0 in 0% DMF (ν_{00} GSB)	0.33	12 ps	0.67	1.1 ns	-	-
Stem loop-3 Δ0 in 0% DMF (ν_{01} GSB)	0.94	35 ps	0.06	800 ps	-	-
Stem loop-3 Δ0 in 0% DMF (S_1-S_N ESA 1)	0.52	1.8 ps	0.28	21 ps	0.20	1.3 ns
Stem loop-3 Δ0 in 0% DMF (S_1-S_N ESA 2)	0.35*	2.2 ps*	0.77	37 ps	0.23	1.3 ns
Stem loop-3 Δ0 in 30% DMF (ν_{00} GSB)	0.43	26 ps	0.57	650 ns	-	-
Stem loop-3 Δ0 in 30% DMF (ν_{01} GSB)	0.86	36 ps	0.14	350 ps	-	-
Stem loop-3 Δ0 in 30% DMF (S_1-S_N ESA 1)	0.42	2.9 ps	0.35	27 ps	0.23	1.3 ns
Stem loop-3 Δ0 in 30% DMF (S_1-S_N ESA 2)	0.20*	4.1 ps*	0.65	37 ps	0.35	480 ps

S7.4 Supplemental transient absorption spectra and timescale fits serial and parallel DNA duplexes

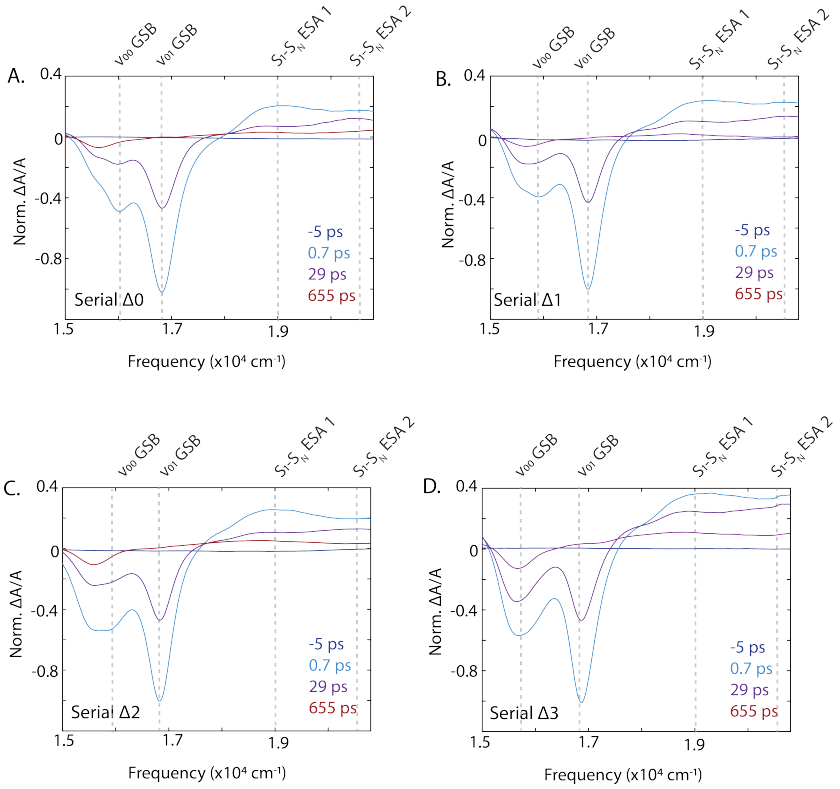

Figure S28. Serial duplex transient absorption. Transient absorption spectra for serial (A) Δ0 (B) Δ1 (C) Δ2 and (D) Δ3 duplex squaraine dimers.

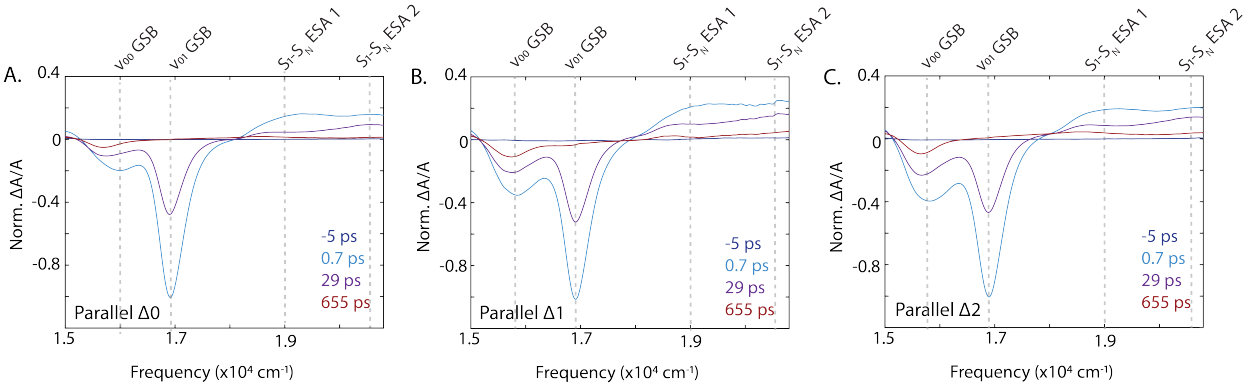

Figure S29. Parallel dimer transient absorption. Transient absorption spectra for serial (A) $\Delta 0$ (B) $\Delta 1$ and (C) $\Delta 2$ duplex squaraine dimers.

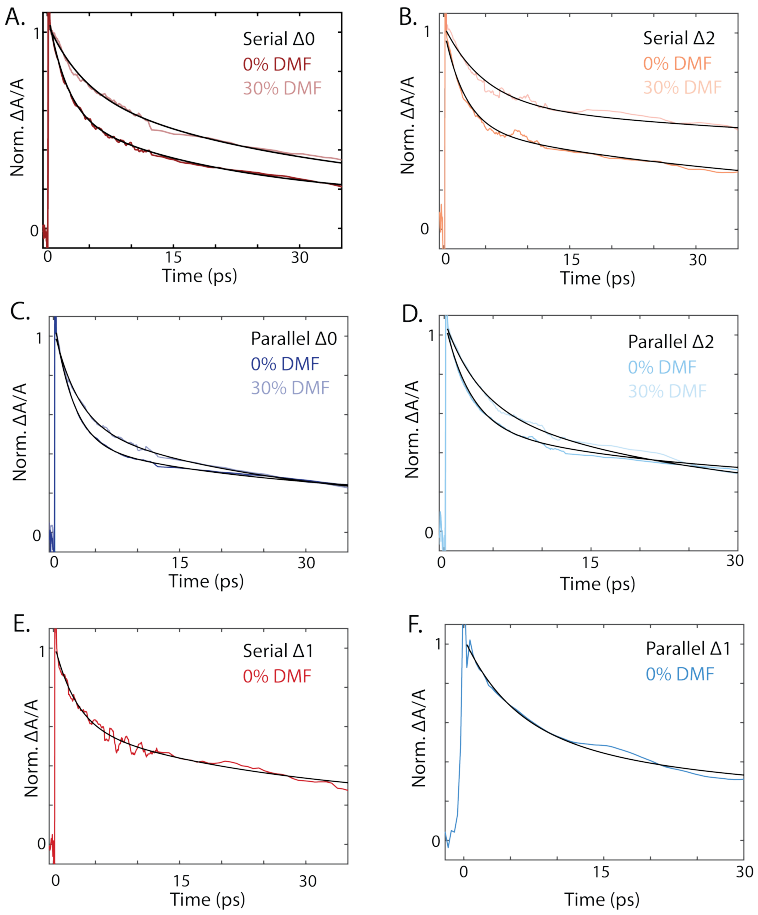

Figure S30. Short timescale ESA kinetics. Transient absorption kinetics of S_1-S_N ESA 1 band. Non-DMF sample shown in solid, 30% DMF sample shown in transparent.

Table S7. Time domain fit parameters for the ESA 1 band in serial duplex transient absorption experiments.

	A_1	τ_1	A_2	τ_2	A_3	τ_3
Serial $\Delta 0$ in 0% DMF (S_1-S_N ESA 1)	0.50	2.2 ps	0.40	27 ps	0.10	1.3 ns
Serial $\Delta 0$ in 30% DMF (S_1-S_N ESA 1)	0.37	4.1 ps	0.53	41 ps	0.10	1.3 ns
Serial $\Delta 1$ in 0% DMF (S_1-S_N ESA 1)	0.43	2.6 ps	0.41	33 ps	0.16	1.3 ns
Serial $\Delta 2$ in 0% DMF (S_1-S_N ESA 1)	0.50	2.5 ps	0.39	45 ps	0.11	1.3 ns
Serial $\Delta 2$ in 30% DMF (S_1-S_N ESA 1)	0.39	4.3 ps	0.26	64 ns	0.35	1.3 ns
Serial $\Delta 3$ in 0% DMF (S_1-S_N ESA 1)	0.37	3.4 ps	0.26	37 ps	0.37	1.3 ns

Table S8. Time domain fit parameters for the ESA 1 band in parallel duplex transient absorption experiments.

	A_1	τ_1	A_2	τ_2	A_3	τ_3
Parallel $\Delta 0$ in 0% DMF (S_1-S_N ESA 1)	0.61	2.3 ps	0.26	41 ps	0.12	1.3 ns
Parallel $\Delta 0$ in 30% DMF (S_1-S_N ESA 1)	0.49	2.8 ps	0.46	38 ps	0.04	1.3 ns
Parallel $\Delta 1$ in 0% DMF (S_1-S_N ESA 1)	0.48	4.5 ps	0.15	19 ps	0.36	1.3 ns
Parallel $\Delta 2$ in 0% DMF (S_1-S_N ESA 1)	0.54	2.6 ps	0.31	45 ps	0.15	1.3 ns
Parallel $\Delta 2$ in 30% DMF (S_1-S_N ESA 1)	0.36	3.3 ps	0.41	46 ns	0.23	1.3 ns

S8 Alternative hypotheses of fluorescence quenching in Serial squaraine dimers

While observed dark state formation observed at the steady state level could arise from intersystem crossing or isomerization, measurement the fluorescence of serial $\Delta 0$ duplexes in different buffer conditions suggests that these processes are not present. In one hypothesis, we posited that strongly coupled squaraine aggregates might be favoring intersystem crossing. H-aggregates can favor phosphorescence due to diminution of the oscillator strength of the singlet state, which allows competing processes to dominate [17, 18]. However, we did not observe any phosphorescence or enhanced fluorescence quenching in argon-saturated solutions of serial $\Delta 0$ duplexes supplemented with Tl^+ or I^- (Supplementary Section S8.1). We also investigated whether the attachment of two squaraine molecules on the DNA strand may have introduced defects on the DNA strand which promoted photoinduced isomerization. While the titration of glycerol, a viscous additive, has led to only slightly enhanced quantum yields, close inspection of the excitation spectra of serial $\Delta 0$ duplexes revealed that the enhancement in quantum yield originates from the increased subpopulation of squaraine monomer-like species in solution, which is likely due to solvation of the squaraine molecules by glycerol (Supplementary Section S8.2). While a number of photophysical processes can give rise to an optically dark state, the lack of evidence that can support the intersystem crossing or isomerization hypotheses further point to the likelihood of charge-transfer state formation.

S8.1 Fast intersystem crossing

Serial $\Delta 0$ duplexes were titrated with increasing concentrations of $TlNO_3$ and NaI to investigate if intersystem crossing is the dominant decay pathway for the serial squaraine dimers. External heavy atoms, for example Tl^+ and I^-, can enhance spin-orbit coupling, which can induce room-temperature phosphorescence [19, 20]. Samples were excited at λ_{exc} = 590 nm while emission spectrum were collected at λ_{ems} = 600–800 nm. For the Tl^+ titrations, no $1\times$ PBS was added to avoid the formation of insoluble Tl_3PO_4. Water and buffer solutions were sparged with argon for 1 hour prior to use. We did not observe any increase in fluorescence quenching of serial $\Delta 0$ duplexes with increasing $[Tl^+]$ or $[I^-]$ when compared to the $1\times$ PBS control, suggesting that intersystem crossing is an unlikely mechanism.

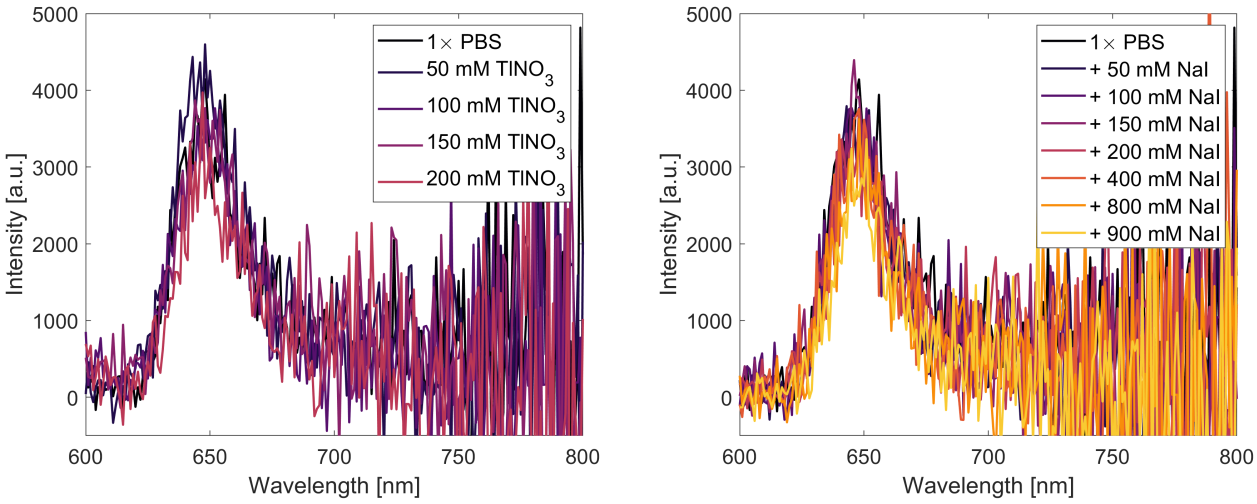

Figure S31. Effect of [Tl^+] and [I^-] on the fluorescence of the serial $\Delta 0$ duplexes. Titration of $TlNO_3$ (left) and NaI (right) in solutions containing 0.5 μM serial $\Delta 0$ duplexes

S8.2 Ultrafast photoinduced isomerization

Cyanines are known to undergo photoinduced isomerization, resulting to very low quantum yields in solution[21]. Restriction of photoisomerization through rigid analogues of cyanine dyes[22] or attachment of cyanines on DNA scaffolds can significantly improve quantum yields[23]. In stark contrast, the quantum yields of squaraine as a free dye and on DNA duplexes are similar which excludes photoinduced isomerization as a potential loss pathway (Figure S32).

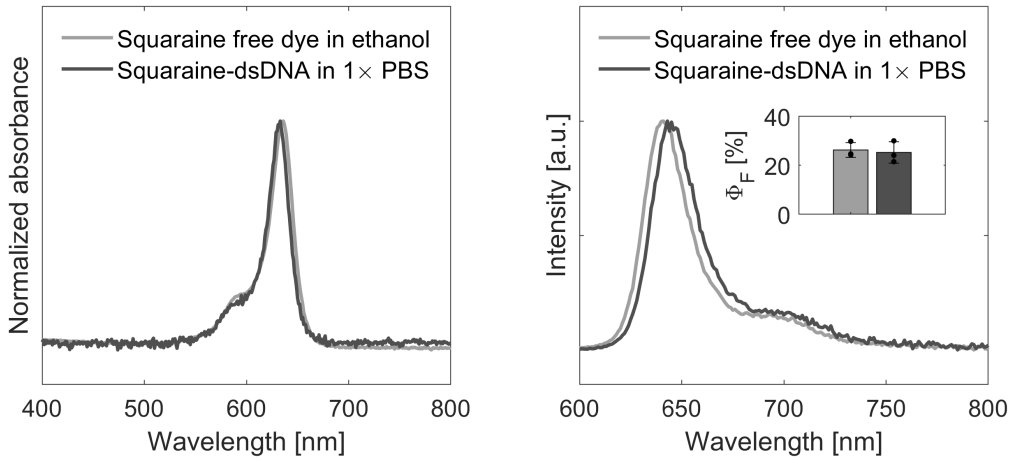

Figure S32. Comparison of steady-state photophysics between free-dye squaraine in ethanol and squaraine attached to DNA (monomer duplex) in 1× PBS. Absorbance (left) and fluorescence (right) spectra (λ_{exc} = 590 nm; λ_{ems} = 600–800 nm). Inset: measured Φ_F for free-dye squaraine in ethanol and squaraine monomer duplex in 1× PBS. Bar height denotes average values while error bars are standard deviations calculated from three independent replicates.

To investigate if our synthetic strategy for squaraine dimers introduced defects on the squaraine-dsDNA constructs that would promote photoinduced isomerization, we titrated glycerol into solutions containing 0.5 μM of serial $\Delta 0$ duplexes. The addition of glycerol into solutions containing squaraine dimer-DNA constructs is expected to increase solution viscosity, which should impede photoinduced isomerization. Increasing volume percentages of glycerol led to increased quantum yields of the squaraine dimer concomitant with the slight reduction in the ratio of the 0–1 and 0–1 intensities. Inspection of the fluorescence action or excitation spectra (λ_{ems} = 710 nm; λ_{exc} = 400–700 nm) revealed

that the increase in Φ_F is due to increase in the subpopulation of squaraine monomer species emitting in solution (Figure S33) rather than emission from the squaraine dimers.

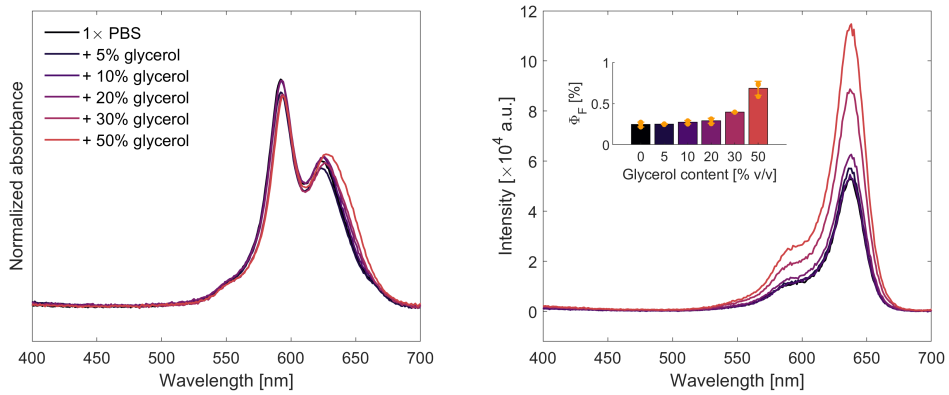

Figure S33. Effect of glycerol content on the steady-state photophysics of squaraine-dsDNA constructs. Absorbance (left) and excitation (right) spectra (λ_{ems} = 710 nm; λ_{exc} = 400–700 nm). Inset: measured Φ_F for serial $\Delta 0$ duplexes in 1× PBS containing different volume percentages of glycerol. Bar height denotes average values while error bars are standard deviations calculated from three independent replicates.

S9 Screening the photophysics of Serial squaraine dimers

In 96-well plates (VWR; catalog number: 82006), squaraine-ssDNA constructs (50 μM) were hybridized with three-fold excess of complementary strands (150 μM) listed in Table S1 in 1× PBS and using a linear annealing temperature ramp: 95°C for 5 minutes then 80–20 °C at −1 °C min^{-1}. The samples were kept at 4°C until further use.

100 l of 1 M of each hybridized squaraine-dsDNA sample was added to each well of a 96-well UV-Star® microplates (Grenier Bio-one; catalog number: 655809). Sample absorbance, emission, and excitation spectra of samples were measured using a Tecan Spark® multimode plate reader. Figure S34 shows the spectra asscociated with the hybridized duplexes and constructs, where the chromophore-containing strand is shown above and listed horizontally, and the complementary strand is listed in the color-coded scheme on the right.

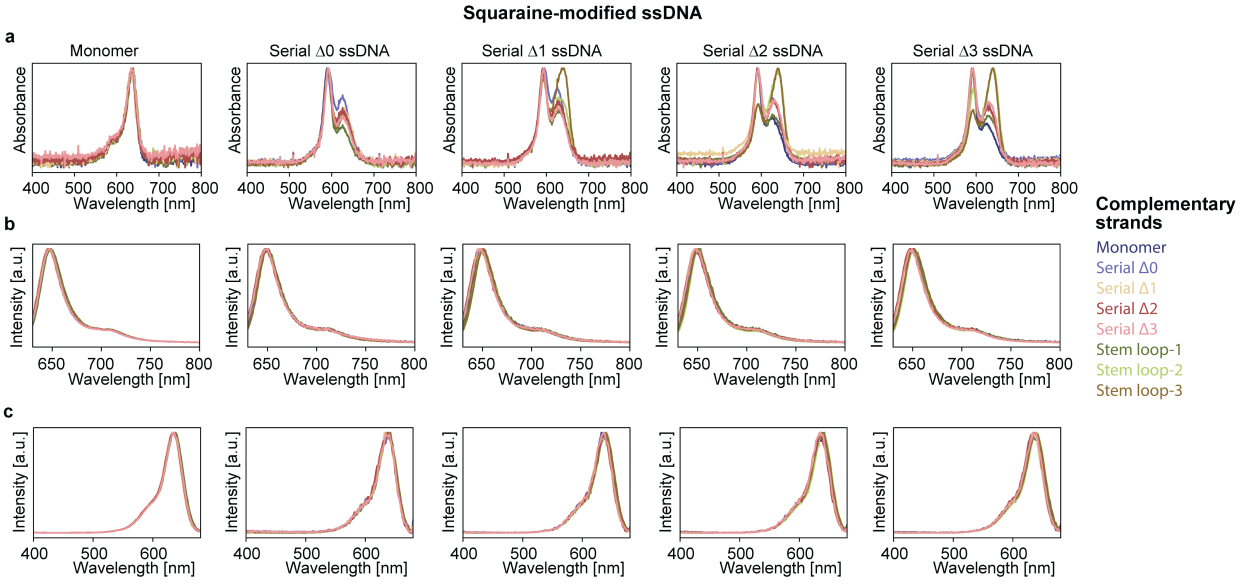

Figure S34. Steady-state spectra of squaraine-dsDNA constructs. Normalized absorbance (**a**), emission (**b**, λ_{exc} = 590 nm), and excitation (**c**, λ_{ems} = 710 nm) spectra of squaraine-dsDNA constructs.

S9.1 Calculating the ratio of 0–0 and 0–1 from absorbance spectra

Absorbance spectra (A_{total}) from Figure S34a were fitted with a two Gaussian model:

$$A_{\text{total}} = A_{0-0} \exp\left(- \frac{(\lambda_{\text{abs}} - \lambda_{\text{abs},0-0})^2}{2\sigma_{0-0}^2} \right) + A_{0-1} \exp\left(- \frac{(\lambda_{\text{abs}} - \lambda_{\text{abs},0-1})^2}{2\sigma_{0-1}^2} \right) + \text{offset} \tag{S16}$$

where A_{0-0} and A_{0-1} are fitted amplitudes for the 0–0 and 0–1 vibronic bands, respectively. λ_{abs} is the absorbance wavelength while $\lambda_{\text{abs},0-0}$ and $\lambda_{\text{abs},0-1}$ are the respective fitted center wavelengths of the 0–0 and 0–1 vibronic bands. The fitted variables σ_{0-0} and σ_{0-1} are the respective standard deviations of the 0–0 and 0–1 Gaussian lineshapes. Table S9 summarizes the calculated A_{0-0} and A_{0-1} ratios.

Table S9. Ratio of A_{0-0} and A_{0-1} calculated from Figure S34a. Absorbance spectra from Figure S34a were fitted with two Gaussian profiles. The resulting amplitudes from the fits were used to calculate A_{0-0}/A_{0-1}. The chromophore containing strand is listed in rows and the complementary non-chromophore strand is listed in columns. Values correspond to hybridized duplexes and constructs.

	Monomer	Serial Δ0	Serial Δ1	Serial Δ2	Serial Δ3	Stem loop-1	Stem loop-2	Stem loop-3
Monomer	3.08	3.00	2.69	3.20	3.28	2.72	2.83	2.86
Serial Δ0	0.55	0.75	0.63	0.59	0.51	0.41	0.56	0.56
Serial Δ1	0.67	0.84	0.68	0.70	0.64	0.62	0.81	1.30
Serial Δ2	0.53	0.75	0.67	0.70	0.73	0.53	1.12	1.81
Serial Δ3	0.46	0.66	0.63	0.64	0.72	0.57	1.45	1.96

S9.2 Relative quantum yield measurements

For microplate-based measurements, relative quantum yields of individual samples were determined using 1 μM squaraine monomers on DNA duplexes (squaraine monomer + Canonical strand 1 in Table S1) in 1× PBS as reference (Figure S32). Relative quantum yields ($\Phi_{\text{F,x}}/\Phi_{\text{F,mono}}$) were calculated as:

$$\frac{\Phi_{\text{F,x}}}{\Phi_{\text{F,mono}}} = \frac{\dfrac{\displaystyle\int_{800\text{ nm}}^{630\text{ nm}} I_{590\text{ nm,x}} \mathrm{d}\lambda}{1 - 10^{-A_{590\text{ nm,x}}}}}{\dfrac{\displaystyle\int_{800\text{ nm}}^{630\text{ nm}} I_{590\text{ nm,mono}} \mathrm{d}\lambda}{1 - 10^{-A_{590\text{ nm,mono}}}}} \tag{S17}$$

where Φ_{F} is defined as the quantum yield of squaraine-dsDNA sample, $I_{590\text{ nm}}$ is the emission intensity when squaraine-dsDNA samples are excited at 590 nm, and $A_{590\text{ nm}}$ is the absorbance of squaraine-dsDNA samples at 590 nm. Subscripts x and mono are identifiers for squaraine-dsDNA samples and the squaraine-dsDNA monomer reference, respectively. Calculated relative Φ_{F} are summarized in Table S10.

Table S10. Relative Φ_{F} of squaraine-dsDNA constructs. Relative Φ_{F} of squaraine-dsDNA samples were calculated using absorbance and emission spectra in Figure S34. The chromophore containing strand is listed in rows and the complementary non-chomophore strand is listed in columns. Values correspond to hybridized duplexes and constructs.

	Monomer	Serial Δ0	Serial Δ1	Serial Δ2	Serial Δ3	Stem loop-1	Stem loop-2	Stem loop-3
Monomer	1.000	1.050	0.960	1.110	1.290	1.890	1.210	1.280
Serial Δ0	0.005	0.005	0.005	0.005	0.005	0.004	0.010	0.010
Serial Δ1	0.004	0.005	0.006	0.007	0.005	0.006	0.030	0.070
Serial Δ2	0.003	0.005	0.007	0.008	0.008	0.004	0.070	0.140
Serial Δ3	0.003	0.005	0.009	0.009	0.010	0.005	0.120	0.180

S9.3 Effect of 30% dimethylformamide

Dimethylformamide (DMF; Millipore Sigma; catalog number: 319937) was added to UltraPure™ DNAse/RNase-Free distilled water (Thermo Fisher; catalog number: 10977015) to obtain 33% DMF in water. Concentrated 10× PBS (Thermo Fisher; catalog number: 70011044) was then added to 33% DMF to obtain a final solution of 1× PBS in 30% DMF, which was used as diluent for all squaraine-dsDNA constructs. Absorbance, emission, and excitation of samples were measured in a Grenier Bio-one 96-well UV-Star® microplates and using Tecan Spark® multimode plate reader. Thermal denaturation curves were measured using an Agilent Cary 3500 UV-Vis from 25 to 90°C at 1°C min^{-1}. Absorbance at 260 nm were measured every 1°C interval.

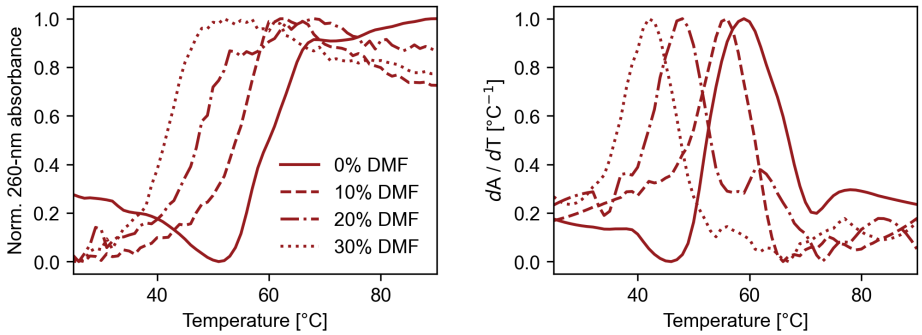

Figure S35. Effect of DMF on the melting temperatures of serial Δ0 duplexes. Thermal denaturation curves measured at different volume percentages of DMF in 1× PBS (left) and corresponding first-derivative curves (right).

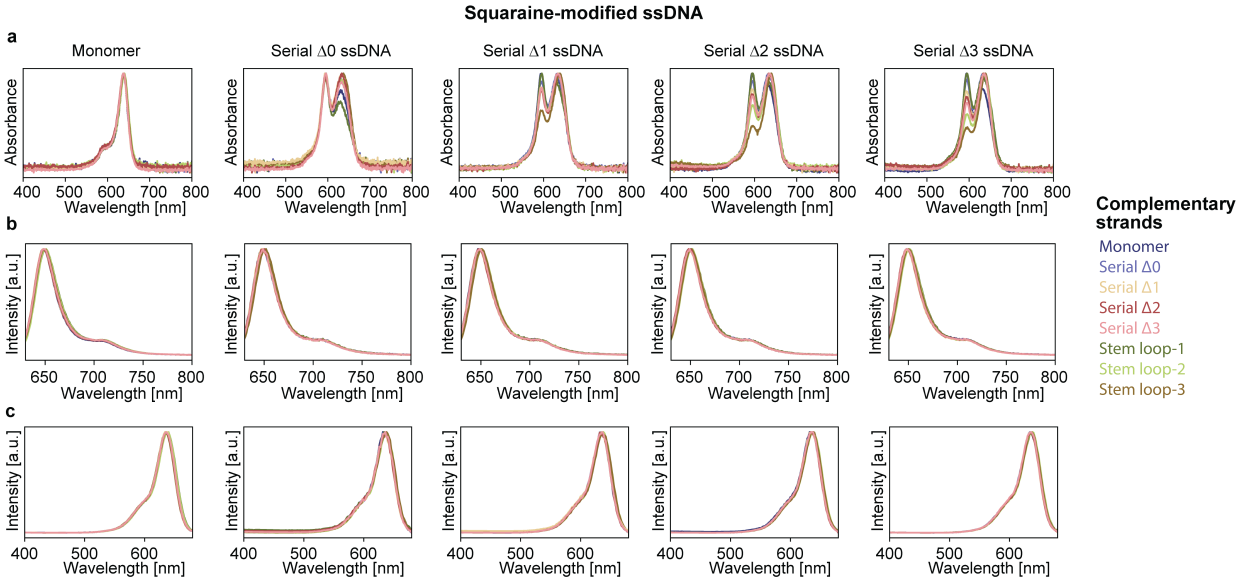

Figure S36. Effect of 30% DMF on the steady-state spectra of squaraine-dsDNA constructs. Normalized absorbance (**a**), emission (**b**, λ_{exc} = 590 nm), and excitation (**c**, λ_{ems} = 710 nm) spectra of squaraine-dsDNA duplexes and constructs.

Table S11. Effect of 30% DMF A_{0-0} and A_{0-1}. Absorbance amplitudes A_{0-0} and A_{0-1} were calculated as described Section S9.1 and using the absorbance spectra of squaraine-dsDNA constructs in 1× PBS in 30% DMF (Figure S36a). The chromophore containing strand is listed in rows and the complementary non-chomophore strand is listed in columns. Values correspond to hybridized duplexes and constructs.

	Monomer	Serial Δ0	Serial Δ1	Serial Δ2	Serial Δ3	Stem loop-1	Stem loop-2	Stem loop-3
Monomer	2.97	3.24	3.11	3.02	3.10	3.06	3.00	3.08
Serial Δ0	0.94	1.07	1.13	1.16	1.06	1.22	1.08	1.25
Serial Δ1	1.10	1.25	1.32	1.38	1.37	1.06	1.41	1.82
Serial Δ2	1.02	1.24	1.36	1.44	1.50	1.09	1.74	2.39
Serial Δ3	0.97	1.22	1.38	1.49	1.60	1.14	1.91	2.44

Table S12. Effect of 30% DMF to relative Φ_F of squaraine-dsDNA constructs. Relative quantum yields of squaraine-dsDNA constructs in 1× PBS in 30% DMF were calculated using the absorbance and emission spectra in Figure S36 and using squaraine monomer-dsDNA construct in 1× PBS. The chromophore containing strand is listed in rows and the complementary non-chomophore strand is listed in columns. Values correspond to hybridized duplexes and constructs.

	Monomer	Serial Δ0	Serial Δ1	Serial Δ2	Serial Δ3	Stem loop-1	Stem loop-2	Stem loop-3
Monomer	0.79	0.75	0.50	0.75	0.77	1.27	1.37	0.87
Serial Δ0	0.02	0.02	0.03	0.03	0.02	0.02	0.04	0.04
Serial Δ1	0.03	0.04	0.04	0.05	0.05	0.03	0.07	0.12
Serial Δ2	0.03	0.04	0.05	0.06	0.06	0.04	0.13	0.22
Serial Δ3	0.03	0.05	0.08	0.07	0.10	0.05	0.18	0.25

S10 Steady-state radical cation spectra by chemical doping

S10.1 Spectrochemical oxidation of squaraine

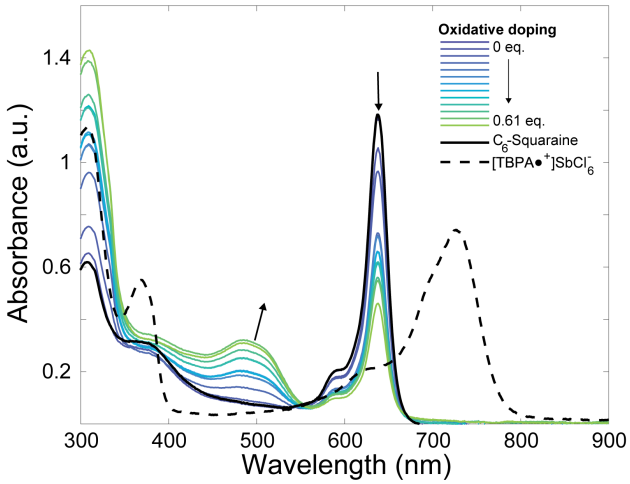

Figure S37. Analytical characterization of squaraine radical cation. Sub-stoichiometric titration of [TBPTA•$^+$]$SbCl_6^-$ into C_6-squaraine 4.57 μM in dichloromethane.

Spectral-analysis of the chemically-oxidized squaraine backbone was adapted from literature using 'Magic Blue' [TBPTA•$^+$]$SbCl_6^-$, where persistant cation radicals of the squaraine family have previously been analyzed.[24] The presence of hydroxyl or phosphate groups in our DNA-squaraine conjugates may result in competing functional group oxidation, squaraine aggregation, and parasitic consumption of the oxidant. Hence, chemically-doping of squaraine was instead achieved using a hydroxyl-free side-chain analogue **C_6-squaraine** which has the same conjugated backbone as all squaraines studied in this work. Anhydrous, argon-degassed CH_2Cl_2 was used as a solvent. CH_2Cl_2 was past through a plug of oven-dried and degassed basic-alumina directly before use. All samples were degassed with argon before for 5 minutes before spectra were recorded in a sealed cuvette.

Consistent with previous observations,[24] we observed a persistent squaraine radical upon one-electron oxidation in CH_2Cl_2 (Figure S37). [TBPTA•$^+$]$SbCl_6$ was titrated dropwise into a solution of C_6-squaraine, samples were briefly shaken before spectra were recorded. The resulting chemical oxidation of C_6-squaraine showed the neutral C_6-squaraine S_0 to S_1 absorption band (575–675 nm) decayed concomitant with growth of a new absorptive feature (425–575 nm) and an isobestic point at 561 nm (Figure S37). These results were consistent with a single state-transfer, with oscillator strength in the same frequency range as the cationic ESA features observed (Figure 4), hence these features were identified as the radical cation of the squaraine. The spectrum shown in Figure 4B was generated by subtracting the 0 eq. spectrum from the 0.61 eq spectrum (normalized to 0-0 band absorbance maximum) to isolate cation specific features.

S10.2 Squaraine Synthesis

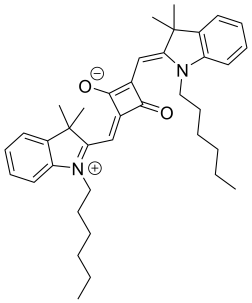

C_6-squaraine was synthesized by adapting literature procedure.[25] 1-Hexyl-2,3,3-trimethyl-3H-indol-1-ium bromide [26] (550 mg, 1.7 mmol, 1 eq.) and squaric acid (80 mg, 0.6 mmol, 0.4 eq.) were dissolved in *n*-BuOH (15 mL) and pyridine (15 mL) and heated at 110°C for 5h. Solvent was removed under reduced pressure. The mixture was redissolved in a minimum volume of CH_2Cl_2 and purified by column chromatography (silica gel, CH_2Cl_2:EtOAc, 9:1 vol/vol). The pure, blue fractions were collected and dried under reduced pressure to yield **C_6-squaraine** as a green-blue solid (555 mg, 1.04 mmol, 61%).

^{1}**H NMR** (400 MHz, $CDCl_3$): δ 7.35 (d, J = 7.3 Hz, 2H), 7.29 (t, J = 7.3 Hz, 2H), 7.13 (t, J = 7.4 Hz, 2H), 6.97 (d, J = 7.8 Hz, 2H), 5.95 (s, 2H), 3.98 (s, br, 4H), 1.85–1.74 (m, 16H), 1.47–1.38 (m, 4H), 1.39–1.27 (m, 8H), 0.88 (t, J = 6.8 Hz, 6H).
^{13}**C NMR** (101 MHz, $CDCl_3$): δ 179.5, 170.0, 142.5, 127.7, 123.6, 122.3, 109.3, 86.5, 49.3, 43.7, 31.5, 27.1, 27.0, 26.8, 22.5, 13.9.
$\mathbf{R}_f$ 0.46 (CH_2Cl_2:EtOAc, 9:1 vol/vol).
FT-IR (ATR) ν = 3442 (br, w, O-H), 2956 (m, C-H), 2927 (m, C-H), 2858 (m, C-H), 1595 (s, C=O), 1482 (s), 1452 (s), 1427 (s), 1354 (m), 1268 (s), 1220 (s), 1171 (s), 1075 (s), 1019 (m), 966 (m), 788 (m).
HRMS (ESI): m/z = 565.3760 $[M + H]^+$; calculated for $C_{38}H_{49}N_2O_2^+$: 565.3789.

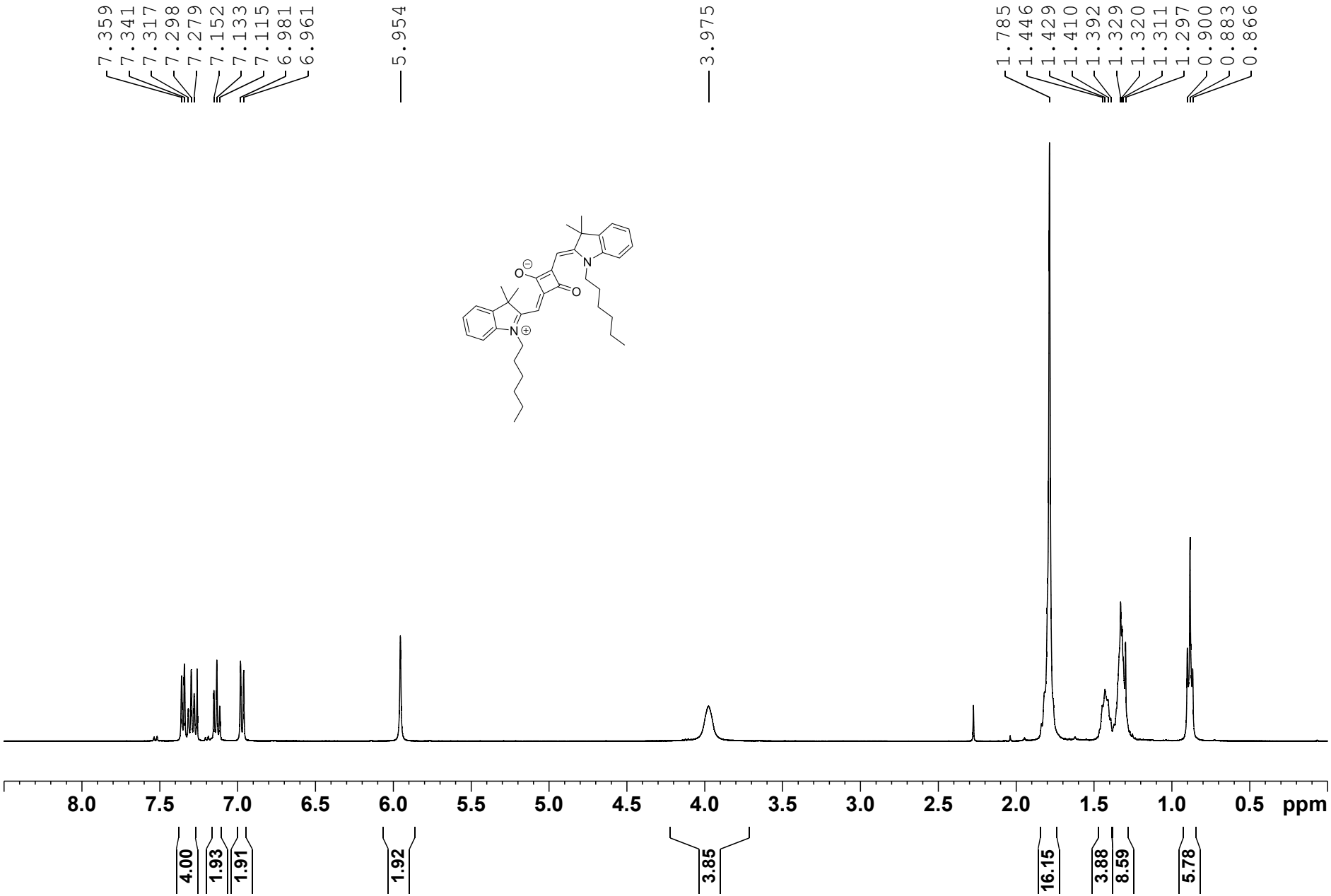
7.359
7.341
7.317
7.298
7.279
7.152
7.133
7.115
6.981
6.961
5.954
3.975
1.785
1.446
1.429
1.410
1.392
1.329
1.320
1.311
1.297
0.900
0.883
0.866
8.0
7.5
7.0
6.5
6.0
5.5
5.0
4.5
4.0
3.5
3.0
2.5
2.0
1.5
1.0
0.5
ppm
4.00
1.93
1.91
1.92
3.85
16.15
3.88
8.59
5.78

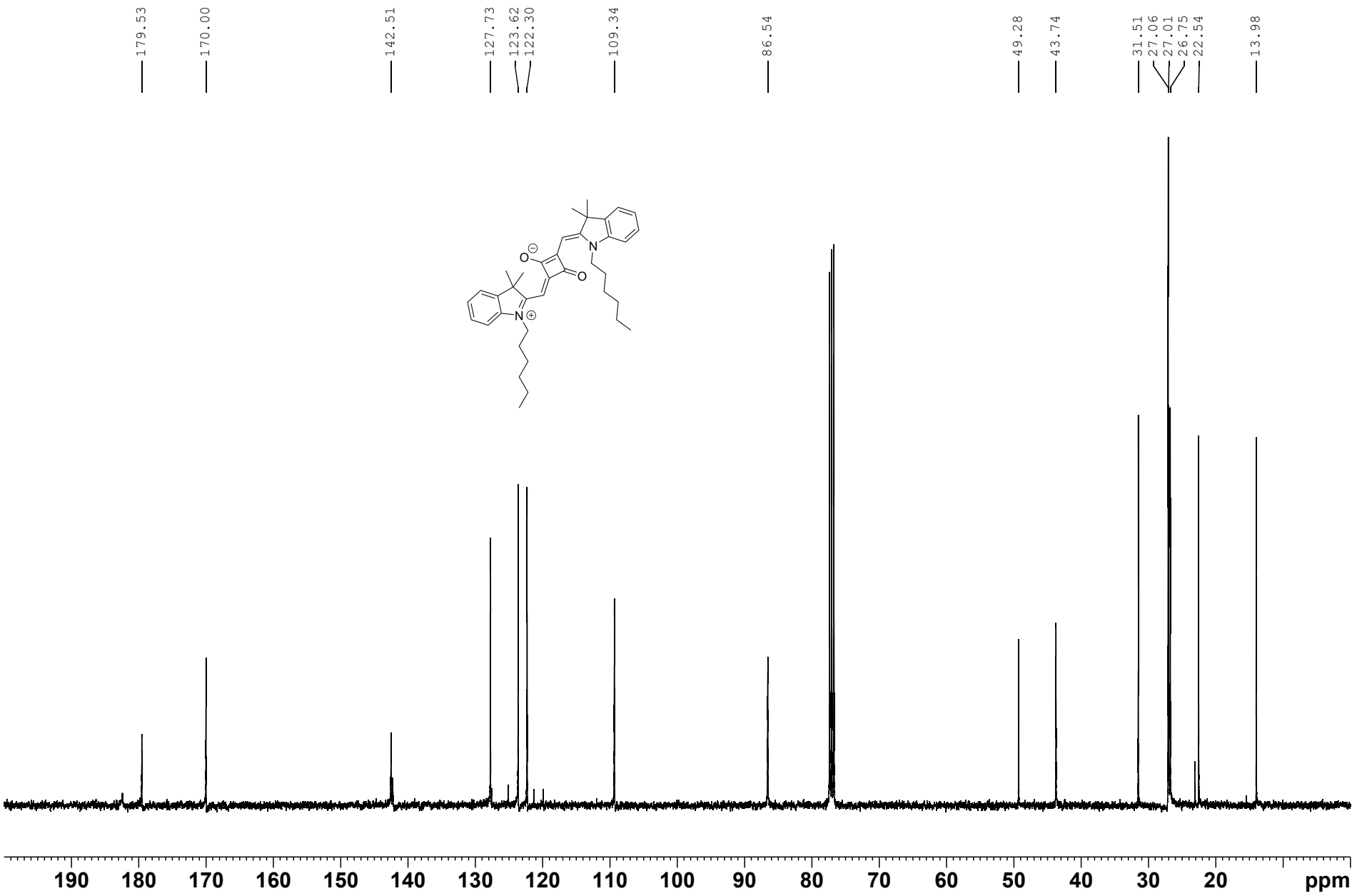
179.53
170.00
142.51
127.73
123.62
122.30
109.34
86.54
49.28
43.74
31.51
27.06
27.01
26.75
22.54
13.98
O
O
N
N
190
180
170
160
150
140
130
120
110
100
90
80
70
60
50
40
30
20
ppm

References

(1) Chang, J. C. *J. Chem. Phys* **1977**, *67*, 3901.

(2) Yamagata, H.; Norton, J.; Hontz, E.; Olivier, Y.; Beljonne, D.; Brédas, J. L.; Silbey, R. J.; Spano, F. C. *J. Chem. Phys.* **2011**, *134*, 204703.

(3) Yamagata, H.; Maxwell, D. S.; Fan, J.; Kittilstved, K. R.; Briseno, A. L.; Barnes, M. D.; Spano, F. C. *J. Phys. Chem. C* **2014**, *118*, 28842–28854.

(4) Avogadro Chemistry Avogadro, version 1.2, 2016.

(5) Shao, Y. et al. *Molecular Physics* **2015**, *113*, 184–215.

(6) Jakalian, A.; Jack, D. B.; Bayly, C. I. *Journal of computational chemistry* **2002**, *23*, 1623–1641.

(7) Wang, J.; Wang, W.; Kollman, P. A.; Case, D. A. *Journal of Molecular Graphics and Modelling* **2006**, *25*, 247–260.

(8) Wang, J.; Wolf, R. M.; Caldwell, J. W.; Kollman, P. A.; Case, D. A. *Journal of Computational Chemistry* **2004**, *25*, 1157–1174.

(9) Michaud-Agrawal, N.; Denning, E. J.; Woolf, T. B.; Beckstein, O. *Journal of computational chemistry* **2011**, *32*, 2319–2327.

(10) Sun, Q.; Berkelbach, T. C.; Blunt, N. S.; Booth, G. H.; Guo, S.; Li, Z.; Liu, J.; McClain, J. D.; Sayfutyarova, E. R.; Sharma, S.; Wouters, S.; Chan, G. K.-L. *WIREs Computational Molecular Science* **2018**, *8*, e1340.

(11) Vendeix, F. A.; Munoz, A. M.; Agris, P. F. *RNA* **2009**, *15*, 2278–2287.

(12) Roux, B. *Computer Physics Communications* **1995**, *91*, 275–282.

(13) Kumar, S.; Rosenberg, J. M.; Bouzida, D.; Swendsen, R. H.; Kollman, P. A. *Journal of Computational Chemistry* **1992**, *13*, 1011–1021.

(14) Grossfield, A. WHAM: The Weighted Histogram Analysis Method, version 2.0.11.

(15) Son, M.; Mosquera-Vázquez, S.; Schlau-Cohen, G. S. *Optics express* **2017**, *25*, 18950–18962.

(16) Cesana, P. T.; Li, B. X.; Shepard, S. G.; Ting, S. I.; Hart, S. M.; Olson, C. M.; Alvarado, J. I. M.; Son, M.; Steiman, T. J.; Castellano, F. N., et al. *Chem* **2021**.

(17) McRae, E. G.; Kasha, M. *The Journal of Chemical Physics* **1958**, *28*, 721–722.

(18) An, Z.; Zheng, C.; Tao, Y.; Chen, R.; Shi, H.; Chen, T.; Wang, Z.; Li, H.; Deng, R.; Liu, X., et al. *Nature Materials* **2015**, *14*, 685–690.

(19) Gaye, M.; Aaron, J. *Anal. Chim. Acta* **1988**, *205*, 273–278.

(20) Wang, J.; Hurtubise, R. J. *Anal. Chim. Acta* **1996**, *332*, 299–305.

(21) Hart, S. M.; Banal, J. L.; Bathe, M.; Schlau-Cohen, G. S. *J. Phys. Chem. Lett.* **2020**, *11*, 5000–5007.

(22) Cooper, M.; Ebner, A.; Briggs, M.; Burrows, M.; Gardner, N.; Richardson, R.; West, R. *J. Fluoresc.* **2004**, *14*, 145–150.

(23) Hart, S. M.; Chen, W. J.; Banal, J. L.; Bricker, W. P.; Dodin, A.; Markova, L.; Vyborna, Y.; Willard, A. P.; Häner, R.; Bathe, M.; Schlau-Cohen, G. S. *Chem* **2021**, *7*, 752–773.

(24) Eberson, L. *The Journal of Physical Chemistry* **1994**, *98*, 752–756.

(25) Markova, L. I.; Malinovskii, V. L.; Patsenker, L. D.; Häner, R. *Org. Biomol. Chem.* **2012**, *10*, 8944–8947.

(26) Bisht, R.; M. K., M. F.; Singh, A. K.; Nithyanandhan, J. *The Journal of Organic Chemistry* **2017**, *82*, PMID: 28121159, 1920–1930.